Credibility-Based Multidisciplinary Design Optimization of Hybrid- and Fully-Electric Aircraft

Nicolas F.M. Wahler*
University of Southampton, Southampton, United Kingdom, SO17 1BJ

Daigo Maruyama†
Technische Universität Braunschweig, Braunschweig, Germany, 38108

Ali Elham‡
University of Southampton, Southampton, United Kingdom, SO17 1BJ

Aircraft designs for future electric aircraft often have large discrepancies in the underlying assumptions for highly influential design parameters. More optimistic assumptions on these parameters could result in better aircraft performance but include higher risks in the realization of the design in the defined timeline. In this work, the novel concept of design credibility is introduced to be used for quantifying the effect of assumptions on the underlying technologies on the design performance and the risks. For a range of highly important parameters, probability curves have been created that can predict a range of assumed future performance by 2035. A credibility-based multidisciplinary design optimization framework is created, which evaluates the maximum achievable mission ranges for hybrid-electric aircraft under credibility constraints. The optimizations are performed using a surrogate-based global optimization routine, the Efficient Global Optimization. With the full framework, the multiple aircraft designs are optimized under a range of credibility limits to create range-credibility Pareto curves. The results show that battery gravimetric energy density is the most dominating factor for the optimization. Motor and airframe parameters have a smaller effect on the achievable range. Their influence on the optimal design depends on the desired credibility level. For high credibilities, the motor is found to be more relevant. For low credibilities, airframe technology improvements are dominant. The shape of the underlying credibility distributions of secondary parameters have a strong effect on their relevance for the optimal configuration.

Presented as Paper AIAA 2023-1847 at the AIAA SciTech 2023 Forum, national Harbor, MD & Online, January 23–27, 2023

*Research Fellow, Department of Aeronautics and Astronautics, Southampton Boldrewood Innovation Campus Building 176, SO16 7QF Southampton, United Kingdom, n.wahler@soton.ac.uk.

†Head of Research Group AI & Machine Learning Methods, Institute of Aircraft Design and Lightweight Structures, Hermann-Blenk-Straße 35, 38108 Braunschweig, Germany, d.maruyama@tu-braunschweig.de.

‡Professor of Multidisciplinary Design Optimization, Department of Aeronautics and Astronautics, Southampton Boldrewood Innovation Campus Building 176, SO16 7QF Southampton, United Kingdom, a.elham@soton.ac.uk.

I. Introduction

In an age where climate change poses a significant challenge for humanity, while at the same time having a constant increase in air travel [1], it is of paramount importance for aircraft to become more sustainable and reduce carbon emissions. With the European Union imposing more stringent regulations on air travel [2], novel technologies are necessary to stay competitive. In this aspect, (hybrid-) electric flight is a promising solution. Hence, the interest in such designs as well as the research effort has increased drastically in the last years.

In current research on the design and feasibility of (Hybrid-) Electric Aircraft (HEA), many assumptions regarding future expected technology levels are made [3–7]. Due to a lack of definite data, often the performance of highly influential design parameters is solely based on predictions of their achievable performance, especially regarding components of the energy network [6, 8]. Thus, these values are highly dependent on the underlying data sources. Predictions and expected values of a parameter can vary widely between different studies. This causes difficulties in the comparison of different aircraft designs and the assessment of the credibility of these predictions regarding their resulting feasibility. In current conceptual design studies, this parameter takes on values between $250 - 1000\frac{Wh}{kg}$ on cell [9] or even pack-level [3, 6, 7]. The current state of the technology achieves energy densities around $200\frac{Wh}{kg}$ [10]. In literature, a cell-level gravimetric energy density of approximately 500 Wh/kg is named as a minimum goal for all-electrical propulsion to become competitive with today's conventional propulsion systems [11, 12]. Some studies acknowledge the uncertainty within their estimations and take it into account, by providing different designs with assumptions for short ($250\frac{Wh}{kg}$) and longer-term improvements ($500\frac{Wh}{kg}$) [6]. Other studies utilize more optimistic assumptions of the attainable energy density for mid- and longer-term, using $700\frac{Wh}{kg}$ [3] or even $650 - 1000\frac{Wh}{kg}$ [7]. In order to attain these energy densities, large improvements in the current state of the art are hence required. However, although this technological performance availability is a key driver in the feasibility of the design, the uncertainty around whether it is an achievable design parameter is rarely taken into account when designing new HEA concepts.

Uncertainties are sometimes considered in qualitative terms, such as by the ICAO defining long term goals for sustainable aviation [13]. ICAO uses the terms *attainability* as a measure of a concept overcoming non-technical barriers, and *readiness* as a degree of achieving technical maturity including overcoming technical barriers [14]. However, both terms are used to evaluate technologies and full designs on a more conceptual scale.

A lack of consideration of whether the proposed technology performance will be available at the time of implementing the design could lead to the design being either unfeasible or sub-optimal, thus diminishing the value of the initial research. Overly optimistic assumptions in which the design parameters are overestimated can lead to scalability problems of a realizable design. On the other hand, conservative assumptions would lead to a more realistic design, albeit with limited scalability and lower economic efficiency. Scalability in this sense is the feasibility of next generation key technologies when applied to different vehicle classes. To address this issue, we introduce a novel concept in aircraft Multidisciplinary Design Optimization (MDO): *design credibility*. We define the design credibility as a measure of the

probability that a design is realizable based on the maturity and performance levels of the underlying technologies. A 100% credible aircraft can only be achieved with current state-of-the-art technologies, which are already available. Any assumption beyond the state of the art will improve the performance, but will reduce the design credibility, as it includes a probability that such an improvement might not be achieved by the targeted time. In their previous publication [15], the authors mathematically formulated the concept of design credibility. Probability functions were developed to quantify the credibility of an electric aircraft based on the state of selected key technologies which have the highest impact on the design scalability.

In this research, credibility-based design optimization is introduced, where the design credibility is defined as a constraint. Such an optimization is used to determine the scalability of full battery electric aircraft with respect to a few key underlying technologies. To achieve this, the study uses credibility predictions initially developed in [15] for the optimization of a Boosted-Turbofan (BTF) regional jet and an electric commuter class aircraft, to evaluate the effect the credibility estimations have on the final design. The aircraft are optimized for maximum mission range under credibility constraints for a range of different optimization formulations. The final results can assess the impact of the performance assumptions for different credibility levels on the final aircraft performance and energy network size. An MDO framework is created with a constrained Efficient Global Optimization (EGO) algorithm using a Bayesian optimization approach at its core. In this approach, Gaussian Process (GP) models are used to predict the objective and the constraint functions as surrogate models. The main advantage of the Bayesian optimization approach using GPs is that only very few sample points are necessary for the initialization of the surrogate models [16, 17]. EGO is a global optimization algorithm that searches the full GP model to evaluate the best locations for new data points to only refine the model at potential minima [18, 19]. It is thus an efficient algorithm to find a global optimum on a GP surrogate with a low number of required additional data points. With the mission simulation as an expensive objective function, using EGO is a promising solution for global optimization at lower computational cost also for higher fidelity optimizations.

Section II defines the credibility criterion that will be applied as well as describe the chosen variables that will be treated as uncertain and their corresponding credibility distributions. Then, the individual parts of the created surrogate-based optimization framework are described in section III. Section IV shows results from the verification process of the individual components used for the optimization. Lastly, section V presents the results of credibility based optimizations under a variety of optimization formulations for two test case aircraft.

II. Design Credibility

A. Credibility Definition

Any prediction of a future event or the future performance of a system is inherently uncertain. The quality and certainty of any predictions depend on a multitude of factors, such as historical developments, steadiness of improvements

and maturity of technology. Accordingly, predictions about the improvement in state-of-the-art for futuristic aircraft designs show a large variability in assumptions. Hence, instead of assuming future performance parameters and using them as deterministic variables, it is reasonable to define probabilistic distributions over these variables, thus treated as stochastic variables, that assign a certain chance of realization to each improvement in performance.

In this research, the concept of design credibility is applied, and the following definition for design credibility is used: *"The probability that at a certain timeframe the technology will have reached at least a certain maturity (performance) level"*. This means the credibility of a parameter is large when the probability that the performance of the technology can exceed the desired value is large. In mathematical terms, this is translated to eq. (1), showing that the Credibility Function (CF) is equal to the complementary Cumulative Distribution Function (CDF) of the parameter.

$$C = P(X > x) = 1 - P(x \leq X) = 1 - CDF \tag{1}$$

The current state-of-the-art performance of a parameter will result in a very high credibility, while a large improvement from this value will result in a low credibility. To assess the credibility of predictions for a parameter, it is hence necessary to define the corresponding Probability Density Functions (PDFs) that define the probable performance range of the parameter for a given time. Their shape is influenced by a range of factors inherent to each parameter and the expected quality of performance predictions. To visualize this approach, an example of this concept is shown in fig. 1. The figure showcases three possible shapes of an underlying PDF (Normal, uniform and exponential distribution shapes) and their resulting credibility functions for a generic parameter. All three distributions have an expected improvement in parameter performance of 3.5% over the status quo. At the current performance level (0% improvement), the credibility is by definition 100%. At the expected value, a 50% credibility level is attained. Further improvements reduce the credibility level. For the shown sample distributions, approximately 0% credibility is attained at around 7% parameter performance improvement for the three distribution shapes.

B. Uncertain Parameters

The goal of this research is to assess and optimize concepts for future aircraft designs for their overall design credibility. Thus, every individual required design input might be considered an uncertain parameter (a stochastic variable in probability theory) and be used in conjunction with a credibility distribution for this investigation.

An assessment of potential parameters for their impact on a viable aircraft design and their projected performance uncertainty from the fields of novel airframe/aerodynamic concepts, propulsion subsystems and energy storage and distribution systems has been performed [20] and credibility curves created [15]. Based on this work, the following parameters are used in this study.

- Gravimetric battery energy density

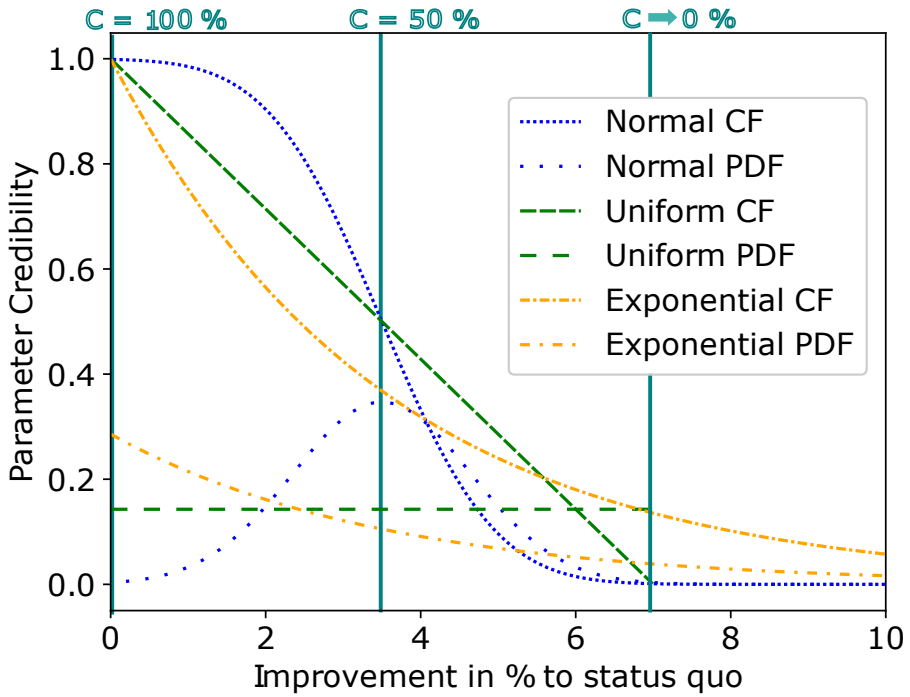

Fig. 1 Credibility function shapes for three different types of underlying probability density functions

- Gravimetric electric motor power density
- Volumetric electric motor power density
- Percentage of laminar flow over the main wing
- Percentage of structural weight reduction due to novel materials and production techniques

All five parameters have a direct and significant impact on HEA designs. They are applicable to a wide range of possible architectures and for aircraft of all sizes. Furthermore, some parameters and their future performances are already well-established in research, while others are still in the laboratory phase. Hence, the approaches to quantifying the credibility will have to be varied for each component, necessitating the establishment of different methods for literature studies and performance predictions. While it can be argued that the selection of only five parameters to set the uncertainty design bounds for a full aircraft is a relatively low number of design parameters, the differences in nature of these parameters will require varied approaches that can easily be extended to further parameters in the future.

C. Method of Parameter Estimation and Curve Fitting

The available data and the level of uncertainty for future performance vary widely between the different parameters. Some parameters, like battery performance, are well-established research areas in literature and have plenty of future performance estimations. The uncertain parameters concerning airframe technologies have low Technology Readiness

Levels (TRLs) at the moment. Thus, direct estimation of the performance and applications by a given time frame are difficult and additional assumptions may be required before it is possible to create credibility curves. Due to this inherent variability of data, each parameter required a bespoke approach in the estimations and curve fitting. Still, the general structure of the approaches is consistent.

As the first step, a thorough literature study on the current state of the art of the parameter is performed, followed by studying estimations of how the performance will improve in the future. This can include finding and evaluating predictions on their accuracy in the past and extrapolations for the future. If it is not possible to find pre-existing predictions, then the credibility curve is used in a less time-specific approach to the potential performance benefits of the technology as a whole. Lastly, a statistical distribution is fitted over the gathered underlying data, and the best-fitting curves are determined based on a statistical test. The specific test used depends on the distribution and plenitude of the underlying data defining the respective distributions.

D. Credibility Curves

The curves were initially created in [15] and the most important parts of this publication are summarized in this subsection. A more detailed explanation of the individual curves, their underlying datasets and the rationale behind the final PDFs is presented in [15].

1. Energy Storage

The estimations for cell-level gravimetric battery energy density are created based on a linear regression of the performance development and predictions over the upcoming years available in the literature. This method makes use of a wide range of predictions on the performance of Li-Ion batteries as an input, yielding more robust results. In the case of the battery, it is expected that technologies based on lithium will remain predominant [12]. However, the chemistry, anode and cathode materials are expected to change paving the way to improved energy densities. Using linear regression to fit the data follows the standard use in literature of this method to forecast Li-ion energy densities [21].

From the interpolations, a set of energy density estimates for the desired year 2035 are derived. Fitting a Normal distribution, a mean and standard deviation are calculated, to define the distribution function [15].

The conversion from battery cell mass to battery system mass depends on the packing method, included system peripherals and applicable safety requirements [21]. Here, a constant scaling factor of $m_{bat,system} = 1.43 \cdot m_{bat,cells}$ suggested for electric aircraft is used [22].

An objective of the credibility curves is to project realistic performance improvements of current trends, confirmed by the nominal projections in [23]. If unexpected developments in battery chemistry, including solid-state batteries should be included in performance predictions, further increases in gravimetric energy density beyond the current

expectations can be derived from the optimistic projections in [23].

2. Electric Machines

Depending on the application, a large range of power is required for the electrification of aviation. The total power required depends on the size of the aircraft [24], as well as power management strategies for hybrid-electric concepts [9]. This can range from small machines acting as booster motors to shave-off power peaks at take-off or cruise, to megawatt-class machines propelling large fully-electric aircraft.

A key parameter for electric machines in aviation is the gravimetric power density. In a recent study, the continuous power density of current electric machines is investigated [25]. The study includes 25 machines from various manufacturers with an average gravimetric power density of 4.072 kW/kg. The machine with the highest gravimetric power density has 8.3 kW/kg.

In order to select the most suitable distribution function for the uncertain parameter, a statistical analysis using the Chi-Squared test is performed. This statistical test examines whether there is a statistically significant relationship between two variables. Since here the empirical data are compared with those of the distributions, the Chi-Squared test is an instrument to measure the goodness of fit of the distribution. The Chi-Square value measures the deviation between the empirical bin counts and the bins that would be projected by the respective fitted distribution function. The smaller the deviation, the lower the Chi-Square value and the better the goodness of fit. The best fit of this data is achieved with a Weibull distribution [15].

The second uncertain parameter characterizing the electric machine is the volumetric power density. The methodology used to create the PDFs is identical to the one used for the gravimetric power density. To establish a uniform basis, the same machines from Bird's study are investigated [25]. Compared to the gravimetric results, it is noticeable that there are outliers in the volumetric power density which have a significantly higher performance than average electrical machines. The reason for this is that these are high-speed machines operating above 20,000 rpm. These machines have high gravimetric and volumetric power densities and also max out at over 8 kW/kg for gravimetric power density. This effect is even more pronounced for the volumetric power density. Compared with other machines, however, it should be noted that the speed is also physically limited and therefore the total power is rather low. Although high-speed machines could be rules as outliers, they were included for the purposes of this study since they provide valuable data points for the technological advancements done in terms of volumetric power density. Again, the Weibull distribution shows the best fit according to a Chi-Squared test [15].

3. Airframe Technologies

The third major part of the credibility distributions considered in this study concern aircraft technologies. Due to the current low TRLs of both technologies and hence a lack of reliable forecast data for an entry-to-service date, a different

approach needs to be taken. For both parameters, an extensive literature study is performed with the aim of finding data points of achieved performance in a laboratory setting, either through flight tests, wind tunnel testing, or high-fidelity numerical simulations. This is done with the underlying assumption that once these technologies have matured enough to be used on new aircraft designs, the achievable range in performance gain will be distributed similarly to current studies on the topic. As such these distributions are not directly related to a specific forecast year but to a forecasted expected performance of the technology.

To find the best fitting statistical distribution, more than 90 continuous functions from SciPy were fitted over the available data and evaluated using the Kolmogorov-Smirnov-test [15]. Due to the scarcity of the data, in this case, the KS-test is preferred over the Chi-Square-test used to estimate the fit for the electric motor parameters as it can be used with sample sizes as small as one per section of the histogram [26]. The Chi-Square-test requires at least 5 points per histogram bar, which would severely distort the shape of the samples.

4. Structural Weight Reduction

Current composite technology has revolutionized aircraft structural design. Modern aircraft such as the Boeing 787 or the Airbus 350 already demonstrated the benefits of large composite structures on aircraft design and structural mass. Composite aircraft structures are currently predominantly built using a tape lay-up process.

Studies for advanced composite lay-up techniques investigate the effects of different levels of freedom regarding the lay-up. A simple method allows the individual plies to be rotated during the layup, allowing better tailoring than the classical 0/45/90 orientations currently in use. Further advances in manufacturing techniques could allow full tow steering. Here, the fiber orientation is constantly varied along the component, either in one or two dimensions [27]. These novel manufacturing techniques have been proven in a laboratory setting, with tow steered coupons achieving significant benefits in strength compared to conventional composite panels [28, 29].

Current studies investigating the effects on wing mass use high-fidelity simulation and optimization techniques to compare mass savings over an optimized wing using conventional layup. Most studies are performed using the NASA Common Research Model (CRM) aircraft model and find mass savings between 5-6% [27, 30, 31] for ply rotations. Using Variable Angle Tow Steering (VAT), the mass saving can increase up to 6-14% [27, 30–33]. The data is best represented by functions of the exponential distribution family. The best representation is found using a Nakagami distribution, a form of generalized Chi-distribution [15].

The baseline for these weight reductions is an optimized wing using conventional composite lay-up techniques. If a metal wing is used as a reference, an additional factor of 20% should be applied [34] to convert to a basic composite structure. For highly aeroelastically tailored composite structures, overall total savings of as much as 40% could be achieved [31, 35].

5. Laminar Flow Estimations

For sustainable aircraft, a further means to improve efficiency is by reduction of aircraft drag. For a large subsonic aircraft, skin-friction drag can amount to up to 50% of the total drag. For laminar flow, skin friction can be up to 90% less compared to turbulent flow [36]. Keeping the flow over the wing laminar can hence yield significant reductions in overall drag. This concept has been extensively applied to low-speed gliders for many years. However, transonic transport aircraft operate at much higher speeds and Reynolds-numbers [37]. Hence, keeping the flow laminar is more difficult to attain. To achieve this, different methods can be employed [37, 38]. The two main research areas are Natural Laminar Flow (NLF) and Laminar Flow Control (LFC). For transport aircraft, LFC is more attainable, as it does not require the airfoil alone to provide extended areas of laminar flow but utilizes e.g. boundary layer suction systems to prevent boundary layer growth and thus a transition to turbulent flow. The technology has already provided promising results, albeit mostly in a laboratory environment. Using LFC over 15-20% of the wing chord for an A340 type aircraft could yield cruise drag reductions of 14% [36]. The LFC is mostly useful in cruise, hence the benefits are larger for long-range aircraft. Different LFC architectures have been developed and tested in wind tunnels, with some also applied to components in flight test aircraft. Flight tests of NLF airfoils have shown laminar flow over 20-45% of the chord [39–42]. Numerical simulations predict higher achievable ranges up to 60% [3, 43, 44]. For LFC, flight tests have shown ranges of 12-65% of the wing chord [41, 45–48], with simulations as high as 85% chord [49–54].

Due to the differences in the achievable laminar area for NLF and LFC, as well as different applicable flight regimes, it is better to have separate curves for the two technologies. Furthermore, the attainable performance depends on the flight regime of the aircraft. A credible estimation needs to be sensitive to this. Thus, as a first step, the data set is split by the laminar flow method; and the associated Reynolds number and sweep angle are determined. This data is used to create multidimensional distributions to take the effect of wing sweep (and by proxy Mach number) and Reynolds number into account as well [55].

Most data points are taken from research regarding larger aircraft in a transonic regime. Hence, the initial credibility curves tend to underestimate performance possibilities for smaller aircraft and at lower speeds/sweep angles. The sweep-Reynolds curves are used as a correction term to increase the credibility of these flight regimes. The higher the wing sweep, and hence the relevant Mach numbers, the better the final points will approximate the original credibility curves [55].

Previous studies into performance limits for both technologies have led to a range of curves estimating the range of flight regimes where either technology can be used sensibly [56, 57]. The curves presented by Hepperle in [56] are selected as baseline for the credibility corrector. The superposition of the data set with the curves shows good agreement if the curves are assumed as mean values for the limits [55]. To create a statistical distribution around Hepperle's curves, the data points are assumed to be normally distributed and mean and standard deviation for sweep-Reynolds-curves for NLF and LFC can be found [55]. From this combined function, a flight condition corrected credibility curve can be

created for any combination of sweep and Reynolds number [55].

For laminarity below 20%, the credibility is very high, as such values can already be obtained with current transport aircraft wing designs. Maintaining laminarity beyond 80% chord is not significant. At those locations, movables such as ailerons or flaps are commonly mounted, and thus the laminar flow is difficult to maintain [38].

6. Resulting Credibility Curves

The credibility curves that have been created from this literature study and curve fitting [15] for all the previously discussed parameters are summarized in fig. 2. The multidimensionality of the laminar flow estimations creates different curves per wing sweep. Here, plots for 10°of wing sweep are presented exemplarily.

III. Optimization Methodology

An MDO framework is created to optimize aircraft under credibility constraints. A global optimization is desired to survey the entire design space. As the mission simulation is an expensive objective function, the goal is to reduce the number of necessary function evaluations to a minimum. Thus, the Bayesian optimization using GP modeling is chosen as EGO framework. The following subsections describe each part of the optimization algorithm and the framework.

A. Gaussian Process

The surrogate model is created using GP regression, a concept of supervised machine learning [16, 17]. A GP approximates an unknown function as a set of random variables that follow a multivariate Gaussian distribution whose mean vector and covariance matrix are expressed by a function m(x) and a covariance matrix parameterized by a kernel function k(x,x'), respectively (eq. (2)). In this model, a Gaussian kernel and a linear expectation function are used for k(x,x') and m(x), respectively. The Gaussian kernel assumes that the output values of the data are smooth on the input variables space and is a sensible assumption for the given problem (eq. (3)). The fitting of the kernel is done by tuning the hyperparameters $\boldsymbol{\theta}$ by maximizing the likelihood function when the sampled data points are given. The number of hyperparameters that need to be fitted depends on the problem dimensionality (D). Own investigations into the quality of created metamodels for the objective and constraint functions have shown that a linear function for m(x) with the shape parameter also being tuned numerically is preferable over a constant or quadratic function with respect to x.

$$f(x) \sim GP(m(x), k(x, x')) \tag{2}$$

$$k(x, x') = exp\left(-\sum_{j=1}^{D} \theta_j |x_j - x'_j|^2\right) \tag{3}$$

The initial sample of the unknown design space to generate the metamodel is obtained using a Sobol-sequence [58].

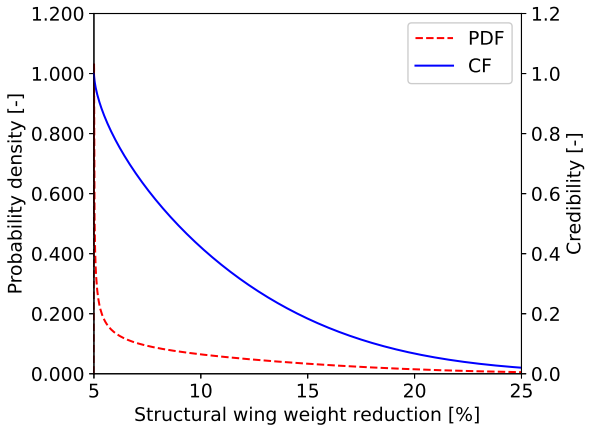

(a) Structural Wing Weight Reductions

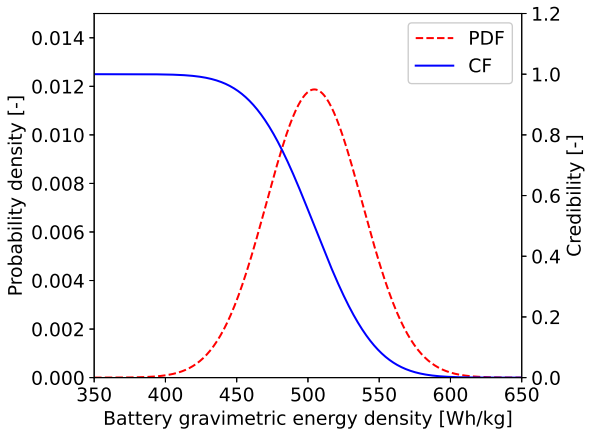

(b) Battery Gravimetric Energy Density

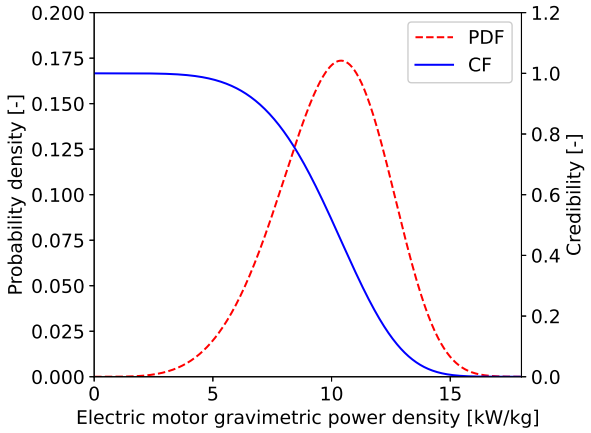

(c) Electric Motor Gravimetric Power Density

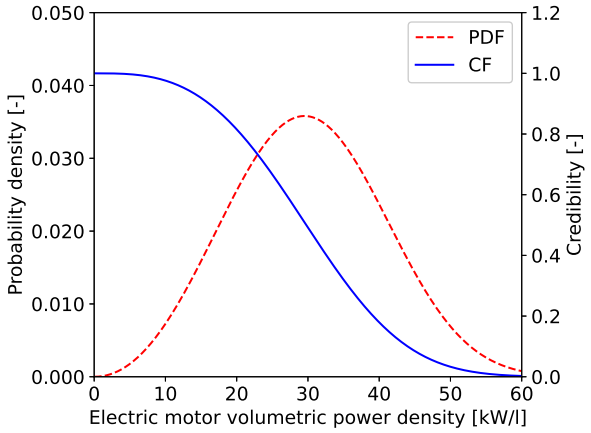

(d) Electric Motor Volumetric Power Density

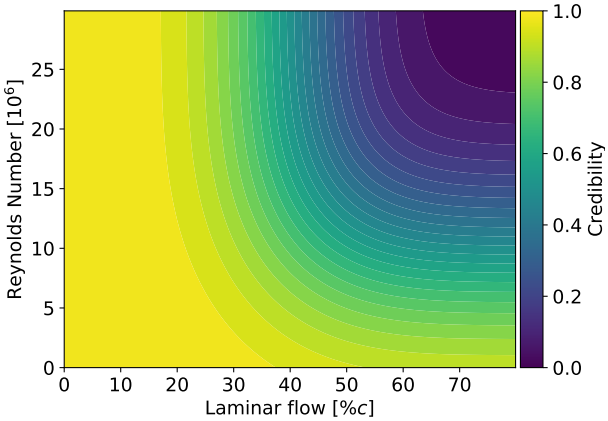

(e) Natural Laminar Flow at 10°Wing Sweep

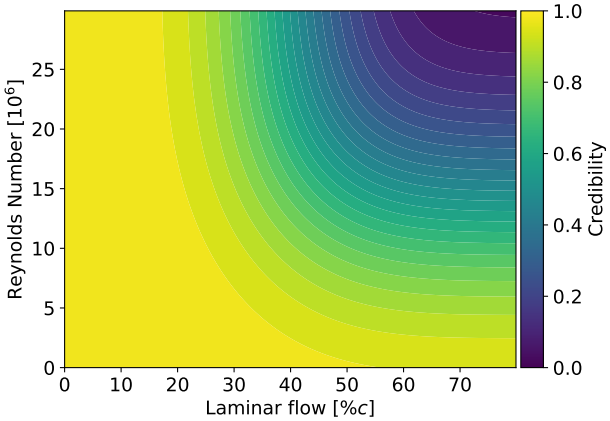

(f) Hybrid Laminar Flow Control at 10°Wing Sweep

Fig. 2 Probability density and credibility functions for the uncertain parameters

The created GP can then be used similarly to an analytical function within the bounds of the sample set. Every obtained data point can be characterized by an expectation and a standard deviation. Hence, the model is not only outputting the

predicted point but also a measure of the certainty level for this prediction. At a sampled point, the standard deviation will be minimal, while in an unsampled area, it will be maximal.

B. Efficient Global Optimization

EGO is an optimization strategy that utilizes the property of the GP to also output a credible interval to evaluate the Expected Improvement (EI) criterion [18], shown in eq. (4). The equation determines the expectation (E) of the improvement (I) over a current minimum point (y_{min}) using the GP's mean ($\hat{y}(\mathbf{x})$) and variance ($\hat{s}^2(\mathbf{x})$), with Φ and ϕ being the CDF and PDF respectively. When the dataset is given, then the predicted mean $\hat{y}(\mathbf{x})$ and variance $\hat{s}^2(\mathbf{x})$ can be obtained by calculating the conditional Gaussian distribution of the GP model.

This criterion is a combination of expectation and standard deviation of the predicted output of the GP and hence is able to both exploit the data set (low expectation) and explore the data set (high standard deviation). The point of maximum EI will be either an optimum candidate or within an unexplored region of the design space, hence potentially yielding a better (unknown) optimum. The so-determined data point is then evaluated with the full model and added to the input data set. The GP model is updated to reflect the inclusion of the new point, and a new candidate point is found until a certain convergence threshold is met. Utilizing this approach, global minima for complex, expensive functions can be found efficiently.

$$\begin{aligned} E[I(x)] = (y_{min} - \hat{y}(x))\,\Phi\left(\frac{y_{min} - \hat{y}(x)}{\hat{s}(x)}\right) + s\phi\left(\frac{y_{min} - \hat{y}(x)}{\hat{s}(x)}\right) \quad if \quad s > 0 \\ E[I(x)] = 0 \quad if \quad s = 0 \end{aligned} \tag{4}$$

The necessary constraints are modeled in a similar way. Instead of an EI criterion, an Expected Violation, or Probability of Improvement (PI), is used (eq. (5)) [17]. This equation calculates the probability (P) of a point's feasibility (F), the difference between a constraint realization ($G(\mathbf{x})$) and the constraint limit value (g_{min}). Analogous to the EI, the function now uses the constraint GP's mean ($\hat{y}(\mathbf{x})$) and variance ($\hat{s}^2(\mathbf{x})$). This estimates the mean and one-sided standard deviation of a point exceeding the constraint boundary and takes on values between 0 and 1. The higher the chance of the constraint being adhered to, the higher this value. The multiplication of EI and PI form the decision basis for the choice of new candidate points.

$$P[F(\mathbf{x})] = \frac{1}{\hat{s}\sqrt{2\pi}} \int_{-\infty}^{0} e^{-[F-\hat{y}(\mathbf{x})]^2/\left(2\hat{s}^2\right)} \mathrm{d}G; \quad F = G(\mathbf{x}) - g_{min} \tag{5}$$

The comprehensive optimization process is described in fig. 3. The optimization algorithm is initialized with a small sample (grey), of which GP metamodels are created (blue). The crucial part of estimating the EI and PI parameters form the core of the optimizer (purple). The adaptive sampling point is then determined by maximizing the acquisition

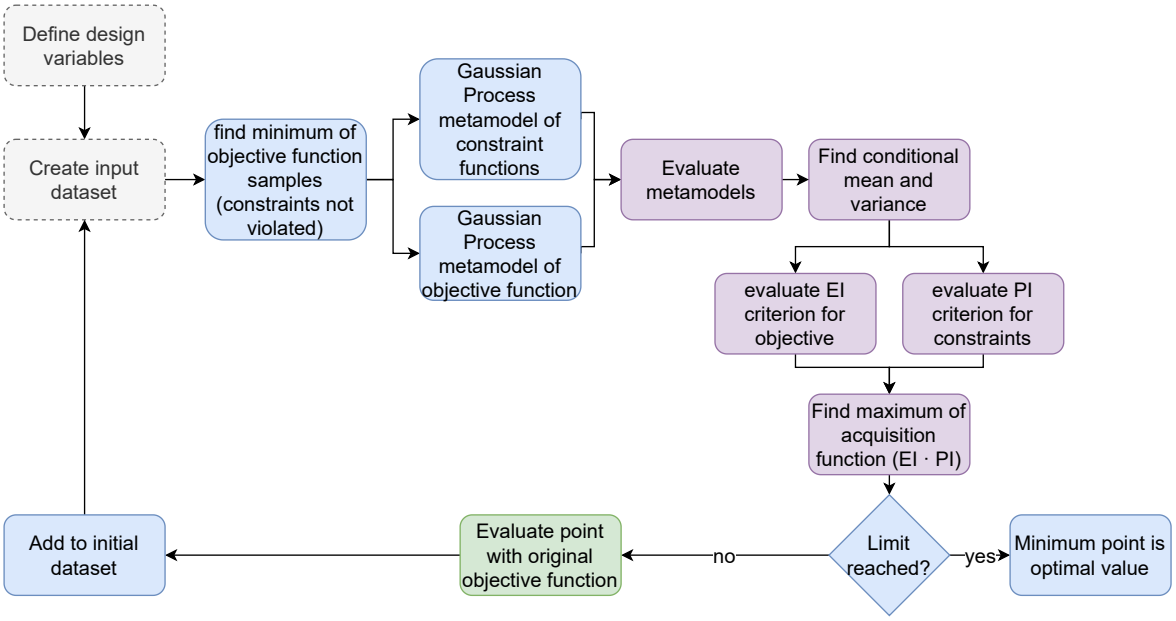

Fig. 3 Flowchart of the EGO implementation used in the optimization framework

function (eq. (6)) which is composed of EI and PI. The PIs thus act as correction terms for the feasibility of a point. If the criterion has not yet found a global optimum, the objective and constraint functions are evaluated again (green) and added to the initial data set. If the EI is zero, a global optimum has been found.

$$x_{new} = \underset{x}{\operatorname{argmax}} \left(E\left[I\left(\mathbf{x}\right)\right] \cdot \prod_{n}^{N_{constraint}} P\left[F\left(\mathbf{x}\right)\right] \right) \tag{6}$$

C. Aircraft Evaluation

The core performance simulation of the aircraft is performed within the SUAVE software [59]. SUAVE is a mission simulation tool created by Stanford University*. The aircraft is modeled through basic geometric parameters as well as a model of the propulsion system. The design mission is divided into multiple individual segments with individual configuration and performance options. Each segment is further discretized, and an iterative solver is used to determine the required thrust and angle of attack to achieve a trim condition for each discretization point. The found thrust and aerodynamic conditions are used to investigate the behavior of the aircraft throughout the full mission. SUAVE also includes a mass breakdown module that estimates the masses of all major aircraft components.

*https://suave.stanford.edu/

D. Energy Network Model

This optimization strongly depends on detailed simulation models of the propulsive and electrical networks. Common energy network models, such as the one implemented in SUAVE and used in conceptual design, are simplistic, accepting a reduction in model fidelity for a low evaluation time. For the optimization studies, a more detailed simulation model for the energy networks in hybrid-electric aircraft is used and integrated into the SUAVE environment [60]. This new network model is able to give higher fidelity simulation results for gas turbine and propeller-driven aircraft. The model also includes more detailed simulations for individual parts of electric networks, such as motors, converters, generators, and energy storage systems. A variety of different machine types, converter topologies, and storage systems are implemented that allow a variety of customization options for the aircraft designer. More detail on the creation of the network models, design options and verification results are presented in [60]. In this study, the full-electric and parallel-electric architectures defined in [60] and shown in fig. 4 are used. With the network, not only the effect of changes in the uncertain parameters can be modeled and assessed, but also the influence of a variety of other relevant parameters for energy network sizing and performance.

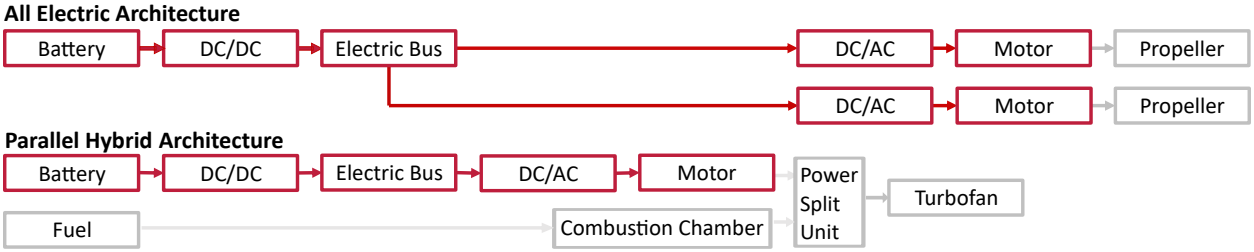

Fig. 4 Individual components of the full-electric and parallel hybrid (BTF) energy network architecture

E. Multidisciplinary Design Optimization Framework

The full MDO framework is shown in flowchart form in fig. 5. Grey boxes denote the necessary initial inputs to create the SUAVE mission simulation environment. Green denotes the mission evaluation and iteration. Lastly, blue refers to all steps taken by the actual surrogate modeling and optimization process.

SUAVE, as a mission analysis tool, will always simulate the mission over the full design range, as well as require as much power from the energy model as the mission simulation requires to converge at a specified flight phase. This can result in physically impossible aircraft, e.g. with negative charges of the batteries in case the mission is longer than the onboard batteries allow, or power requirements that can exceed the maximum power available. This would make creation of a smooth surrogate difficult. To avoid calculations with a large number of physically impossible aircraft, an internal iterator is added into the SUAVE model that only passes converged/feasible designs to the optimizer.

The internal iteration loop simulates the given mission and computes the aircraft performance, including energy requirements for the full mission. It then applies a mass breakdown of the aircraft components to check if the aircraft is

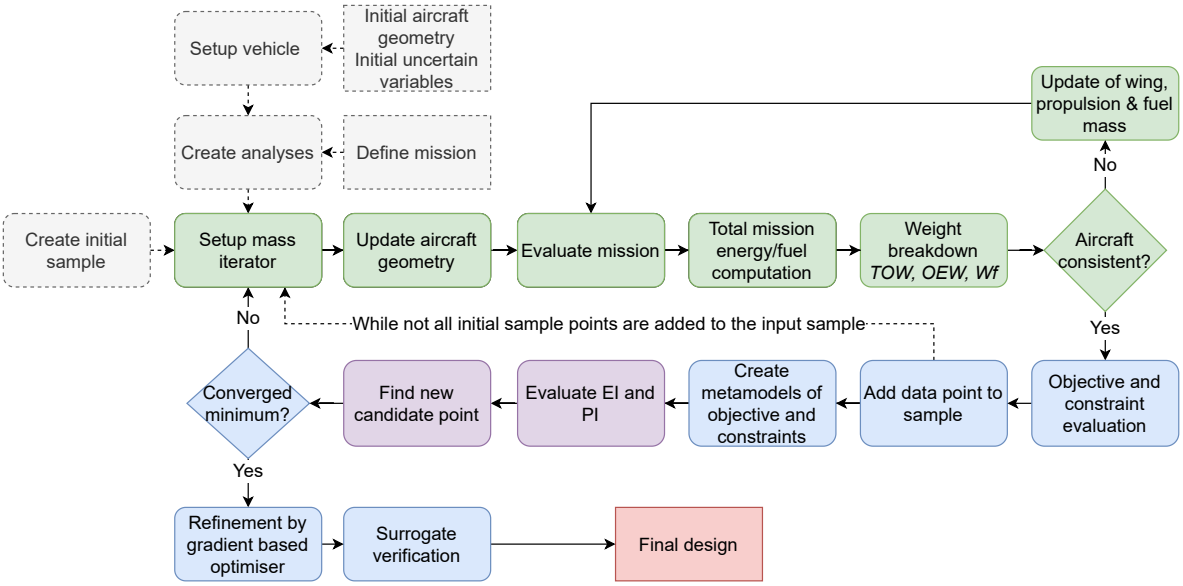

Fig. 5 Optimization procedure flowchart

consistent mass-wise for the flown mission. If not, then the energy network is resized based on the required mission energy for the battery mass and the initial design point power loading for the engines. To account for changes in the Maximum Take-Off Mass (MTOM) of the aircraft, the wing is also resized in accordance with the initial design wing loading. Resizing the wing and engine with the original design point's specified wing and power loading assures that the overall aircraft design point does not change within the iterations.

Once the aircraft is converged, the data point is stored as a sample point. Before the actual optimization takes place, an initial sample is generated for the creation of the initial metamodels. Within the iteration loop, this new sample point represents the chosen new point according to a maximized EI/PI criterion. While an EGO approach will eventually converge to the global minimum of the (constrained) design space, it is not known a-priori how many additional sampling points are required. Hence, a more efficient approach is used. For both initial and adaptive sampling, the number of sample points is prescribed. The total number of infill points is variable and depends on the aircraft type and exact optimization formulation. However, generally a split of 1:2 between the initial sample and infill points [17]. On the final refined metamodel, a gradient-based optimizer is then used to improve the resulting minimum. As the metamodel is an analytical function, this gradient-based optimization is very fast. Lastly, as the resulting optimum point is not necessarily a sampled point anymore, the quality of the metamodel at this point is verified by confirming that the final optimum is approximated well and that all constraints are adhered to properly.

IV. Verification

Following the creation of the methodology for the optimization and the creation of the optimization framework, the next step is a thorough verification of the created codes. The nature of an optimization framework makes a validation with experimental or real-world data difficult. Hence, operational status of the full framework is proven through a series of unit and system tests as appropriate.

The mission simulation software SUAVE and its components was extensively tested and verified by the creators at Stanford [59, 61], and is not further investigated in this article.

This chapter will describe the verification efforts undertaken to verify the implementation of the energy network models and the mass modeling in SUAVE against a reference aircraft design. The pure implementation of the EGO algorithm is tested against analytical test functions. Lastly, the coupling of EGO and SUAVE is tested against a gradient-based optimization routine within the optimization setup provided by the SUAVE software itself.

A. Verification Against Initiator Design

To verify the integration of the energy network with SUAVE, a verification against a design created by TU Delft using their well-verified in-house tool Initiator [62] is chosen. A good agreement with the TU Delft design is particularly of interest as all aircraft described, used, and optimized in the later sections are originally designed with this tool. However, it has to be kept in mind that the two tools have differences in the methods and fidelity of individual modules. SUAVE actually simulates a full engine cycle with individual parts for turbine and compressor stages. Initiator only has simple statistical relations. Initiator can vary power splits of hybrid architectures and flight speed/climb rates continuously throughout a mission. SUAVE needs to discretize the mission in small sub-segments of constant speeds and boost motor power.

The aircraft shown in fig. 6 is a 50 passenger BTF regional jet. It is designed according to CS-25 regulations with a design range of 500 NM at a cruise speed of M0.7. Contrary to the SUAVE implementation, a mission segment in the Initiator is prescribed by a throttle setting and thus speeds and climb rates vary. For the implementation with SUAVE, the climb and descent segments are discretized into three segments each. The Initiator boosting strategy for the electric motors is prescribed as a fraction of total propulsive power. This is converted to corresponding fractions of total available motor power for the SUAVE implementation.

The results of the SUAVE mission simulation and the TU Delft results are shown in table 1. The SUAVE aircraft uses less total energy over the mission, visible by a lower battery and fuel mass. This leads to reductions in the Operational Empty Mass (OEM) and MTOM. The structural masses are similar, indicating that the mass estimations based on geometric parameters are similar. The propulsion network used by the Initiator is simple, similar to other networks currently used in conceptual design. Thus, variations in the network performance, resulting battery mass and fuel requirements are expected due to the differences in fidelity, which will manifest themselves in different total mission

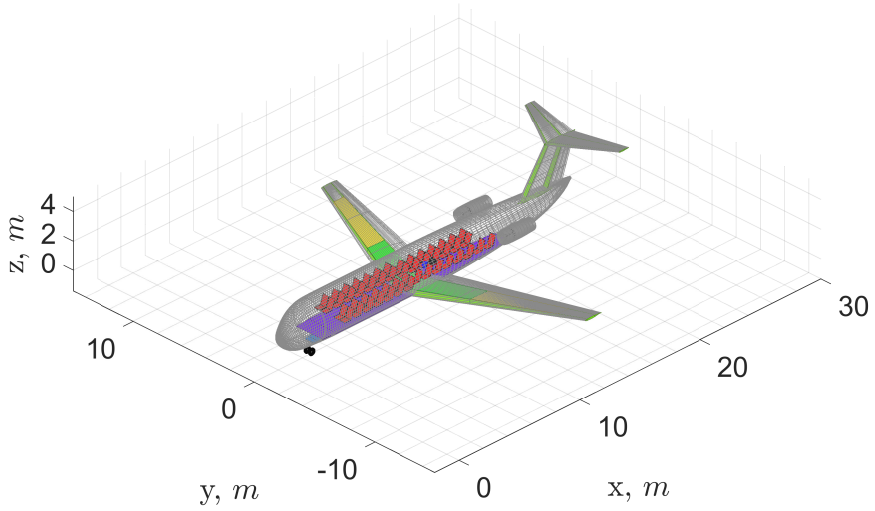

Fig. 6 Initiator designed BTF regional jet

energy consumptions.

Table 1 Comparison of TU Delft Initiator values and SUAVE simulation results

Parameter	Initiator [t]	SUAVE [t]	Difference
Payload	5.3	5.3	0
Battery	10.5	10.0	- 5.1 %
Fuel	2.07	1.89	- 8.6 %
OEM	28.4	29.5	+ 3.9 %
MTOM	35.7	36.7	+ 2.6 %

Overall, the values show good agreement between the two models and indicate that SUAVE and the network model are working well within the inherent limitations and uncertainties of conceptual design methods.

B. Optimization Verification

The implemented optimization algorithm has been verified against multiple analytical functions with known minima. Here, the results of a constrained optimization using the Branin-Hoo function are shown. The Branin-Hoo function has three global minima and is shown in equation 7. It is a common and well-suited function for verifications of global optimizers as it has multiple global minima [17].

$$f(x) = \left(x_1 - \frac{5.1x_0^2}{4\pi^2} + \frac{5x_0}{\pi} - 6\right)^2 + 10\left(1 - \frac{1}{8\pi}\right)cos(x_0) + 10 \tag{7}$$

Figure 7 shows the true reference function. The three global minima are well visible. To test if both EI and PI

criteria work properly, two constraints are imposed as shown in fig. 8. The blue area shows the feasible design space where both constraints are satisfied.

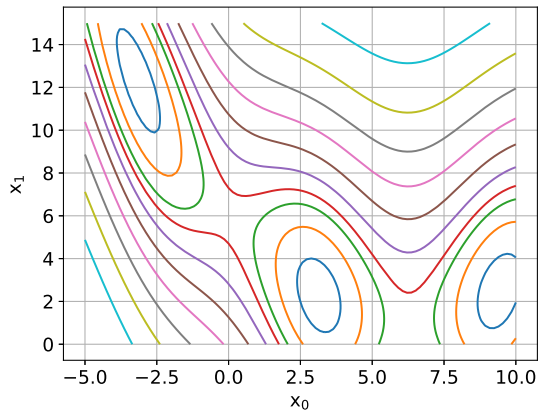

Fig. 7 True objective function (Branin-Hoo)

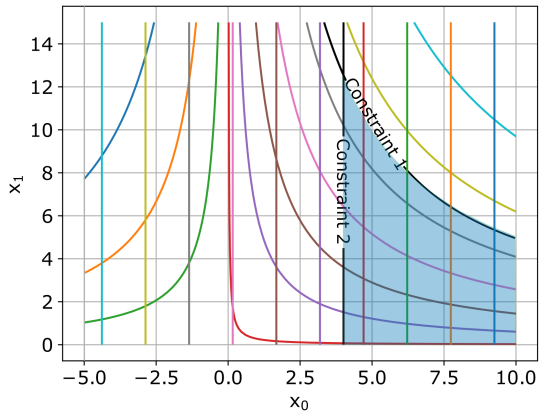

Fig. 8 Constraint functions (satisfied in blue area)

The improvements of the GP-based objective function metamodel being refined by EGO-based new sample points are shown in fig. 9. Starting off with an initial metamodel after 8 sample points, neither the final shape nor any optimum is represented well. After 5 additional points have been added, significant improvements in the model are visible. At 9 additional points, the function is already well modelled, and at 14 points, the constrained optimum is found to machine precision. Furthermore, it can be seen that even though additional samples are only added in the feasible subspace, the quality of the model is visibly improved over the full design space. Differences in the numerical contours between fig. 7 and the final shape in fig. 9 are due to differences in the input data of the full metamodel due to the sampling, but have no influence on the actual minimum. These differences show that the metamodel is not perfectly refined outside of the optimum, and will increase further away from the highly sampled area around the minimum.

C. Verification Within SUAVE

Following successful verification of the optimization framework on a simple test function, the framework is integrated into the SUAVE environment. The implementation verification test case is a conventional turbofan regional aircraft which will be optimized for fuel burn on a typical mission with wing area and cruise altitude as design variables. A constraint is imposed that the total available fuel mass must be larger than the fuel burnt during the mission. The given aircraft and mission are not changed, and solely the optimizer is replaced for an equal comparison. The resulting design space based on a grid of SUAVE simulations is shown in fig. 10. Figure 11 shows the resulting GP metamodel initialized with 8 samples and after 10 further function evaluations.

At only 18 total data points, the optimizer has converged to the global optimum and the resulting metamodel has an error of less than 1% at the optimum value (model: 6953 kg vs. true: 6949 kg).

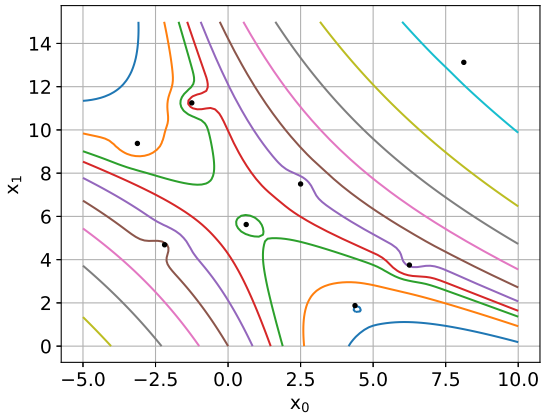

(a) Initial objective metamodel using 8 sample points

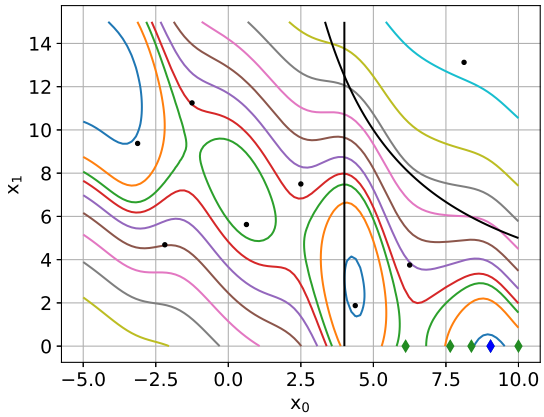

(b) Objective metamodel after 5 additional samples

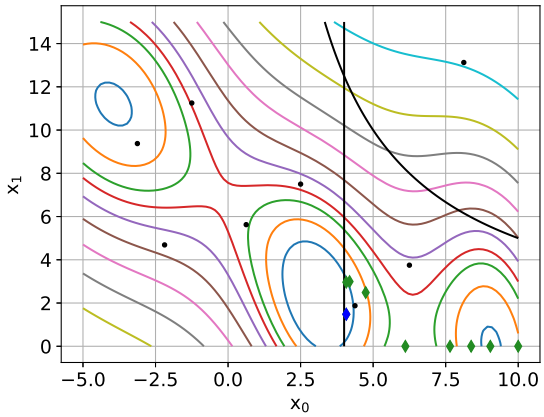

(c) Objective metamodel after 9 additional samples

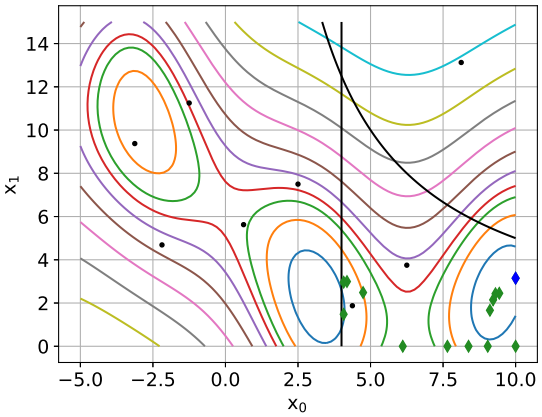

(d) Objective metamodel after 14 additional samples

Fig. 9 Improvement of the objective metamodel with the infill sampling strategy considering the constrained design space

V. Test Case Optimization Results

This section shows the results of two aircraft case studies that are optimized for maximum mission range under a range of credibility constraints. The results showcase the impact of different optimization formulations and feature discussions on the relative importance of the uncertain parameters defined in section II:

- Natural Laminar Flow (NLF)
- Structural Weight Reductions (SWR)
- Battery Gravimetric Energy Density (BGE)
- Electric Motor Gravimetric Power Density (EMG)
- Electric Motor Volumetric Power Density (EMV)

The aircraft are optimized for four levels of average credibility, 30%, 50%, 70%, and 90%, under different optimization formulations, and with varying sets of uncertain parameters. These levels are chosen to showcase changes

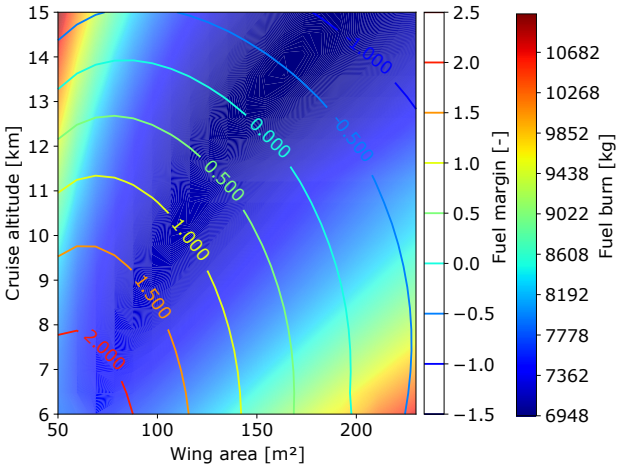

Fig. 10 SUAVE design space visualization by full factorial grid search

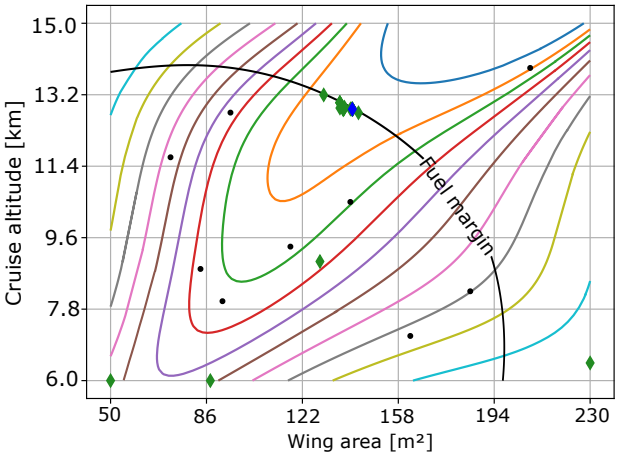

Fig. 11 Resulting metamodel obtained through EGO process with limiting fuel margin constraint

for low/medium/high levels of credibility, and to show how parameter influences change along different credibility levels. The objective is to showcase applications for credibility criteria, how different subsets influence relative importances, and how the underlying credibility function curves influence the results.

A. CS-25 50-Passenger Boosted-Turbofan Regional Jet

The first case study considers a regional aircraft. The aircraft is designed with 50 seats and a twin BTF layout. Figure 6 shows the initial design that was created at TU Delft using their in-house tool Initiator [62], using the same process as described in the previous subsection. Table 2 gives some key design parameters characterizing the baseline aircraft. The BTF layout required some changes in the SUAVE setup compared to the Initiator baseline. The Initiator computes the respective motor boost power for each mission segment as a fraction of the total propulsive power. The SUAVE network implementation does not allow for this split, as the total propulsive power at a certain point along the mission is the final output of the whole network operation. The SUAVE model requires a constant motor boost power as fraction of maximum rated motor power per mission segment. Thus, for every segment of the original mission that is discretized for the SUAVE simulation, an equivalent average boost power that is constant throughout the segment is computed. This value is converted into fraction of maximum rated power and used as a constant for the respective flight phase.

In this study, the optimization goal is to maximize the achievable mission range of different HEA while staying within certain mass or wing span limits. As design variables for this optimization problem, only the previously described uncertain parameters and the mission range are used.

The credibility is passed to the problem in the form of a set of individual component credibility constraints (C_i). The leading parameter for the assessment is average credibility ($C_{avg,limit}$). Individual component credibilities are

Table 2 Key design parameter of the BTF regional jet for the optimization

Parameter	Value
Wing loading	4682.3 N/m^2
Thrust-to-weight ratio	0.193
Electric motor power loading	0.0677 N/W
Number of passengers	50
Cruise speed	207.6 m/s
Cruise altitude	10668 m
Wing aspect ratio	8.43
Wing taper ratio	0.32
Wing sweep	22.5°

allowed to be lower than this value, with limits set to 10% less. These constraints force a trade-off between the uncertain parameters while limiting the allowable decrease in credibility. This prevents large spreads of individual credibility values, which would still have an acceptable average result, which in turn reduces the inherent credibility of the overall optimization results. This could happen, e.g., if one parameter optimizes to a very low component credibility while all other parameters optimize to high credibilities. The average would be within its respective limit, yet the overall design credibility would still be low due to the singular low value. The final results will show a Pareto front of the maximum mission range ($R_{mission}$) versus average credibility for the given aircraft. With the use of an internal iterator taking into account necessary consistency requirements for a physically possible design, the final optimization problem to be solved by the EGO can be stated as shown in eq. (8).

$$\begin{aligned} min \quad & -R_{mission} \\ s.t. \quad & b \leq b_{max,ICAOgate} \\ & C_i \geq C_{i,limit} \qquad \forall i = 1, 2, ..., n \\ & \frac{1}{n}\sum_{n=1}^{i} C_i \geq C_{avg,limit} \end{aligned} \tag{8}$$

The aircraft is constrained by a maximum wing span limit ($b_{max,ICAOgate}$) to adhere to the respective ICAO gate category. Due to the fixed design point in the internal iterator, for a fixed-wing geometry, this is equivalent to a MTOM constraint and will be visible as such in the result analyses. If wing geometry parameters are added as design variables, a further constraint on the maximum fuel burn ($W_{fuel,limit}$) is implemented to ensure that aerodynamic efficiency is equal or higher for an optimized result over an aircraft of the same credibility level without an optimized planform. Furthermore, the wing span constraint is changed to a mass constraint to allow fair comparison between all optimization cases for this aircraft. The MTOM limit ($MTOM_{max}$) is set equal to the resulting limiting MTOM

from the fixed-geometry optimizations. For the described case of a CS-25 aircraft and variable wing geometry, the full optimization formulation when using wing geometry as design variables is given in eq. (9). Trade-offs between the uncertain parameters at different credibility levels will influence the internal mass distribution between the performance parameters. changes in the component masses result in the resizing the batteries and fuel capacities, and thus the achievable mission ranges. While lower design credibility will always allow an increase in range due to higher individual parameter performance, the optimal internal distribution resulting in the highest gains needs to be found through a numeric optimization.

$$\begin{aligned} min \quad & -R_{mission} \\ s.t. \quad & MTOM \leq MTOM_{max} \\ & W_{fuel} \leq W_{fuel,limit} \\ & C_i \geq C_{i,limit} \qquad \forall i = 1, 2, ..., n \\ & \frac{1}{n}\sum_{n=1}^{i} C_i \geq C_{avg,limit} \end{aligned} \tag{9}$$

For each of the uncertain parameters as main inputs, the bounds are set such that the lower bounds exceed the credibility constraint limits. The upper bounds are set high enough to still obtain a sensible aircraft yet not limit the final optimized results. The mission range is a necessary input parameter as SUAVE simulates a fixed flight distance. Hence, this parameter must be explicitly given as an input to the optimizer. The objective function directly uses this input value without further conversions. Again, the bounds are found experimentally such that neither has an impact on the final result. Any further necessary constraints or assumptions to assure a realistic aircraft are taken care of by an internal aircraft iterator.

The BTF aircraft was optimized for four levels of average credibility, 30%, 50%, 70%, and 90%, under three different optimization formulations. The first case optimized only the parameters pertaining to the electrical network. The second set of optimizations utilized all uncertain parameters. The third optimization case introduced the wing geometry parameters as additional design variables to concurrently optimize the wing and credibility for a further improvement in aircraft performance. Allowing changes in the wing geometry will not only change the internal mass distributions but also influence the aerodynamic performance on the aircraft, allowing further improvements in achievable mission range. The first two optimizations use the formulation given by eq. (10), replacing the MTOM limit with a limit on the wing span (ICAO class C). The third optimization uses the formulation given by eq. (9).

The results shown in fig. 12 are normalized relative to the reference aircraft (fig. 6) performance. The reference aircraft was designed using common values in the electric aircraft design literature as inputs for the uncertain parameters.

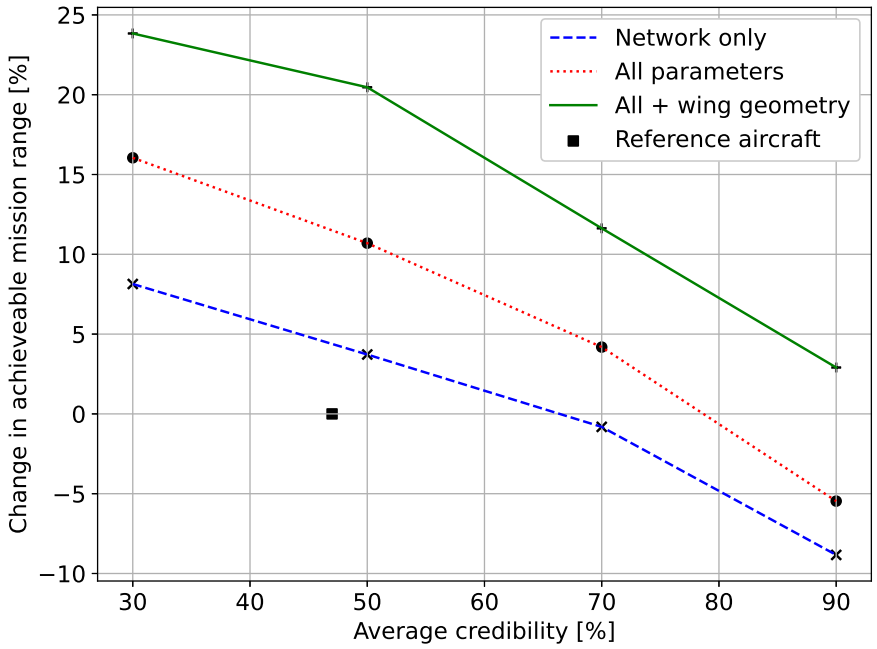

Fig. 12 Credibility-mission range Pareto front curves for the regional jet optimizations

For a comparison with the optimized aircraft results, its performance, as modeled in SUAVE, is shown in the leftmost column of the following tables. As the aircraft was transcribed into the SUAVE format with the accompanying assumptions on the mission profile, the performance differs compared to the original Initiator result, but is consistent within the SUAVE simulations and thus the optimized aircraft results.

Comparing the curves, the more design variables are added to the optimization, the better the overall performance of the resulting aircraft. The relative change in mission range between highest and lowest credibility is ca. 17% for the network only case, while the other two cases using all five design variables have a relative change of ca. 21%. Thus, despite an absolute performance benefit, the combination of uncertain and wing geometry as design parameters has only a small impact on the relative performance difference between different credibility levels. Furthermore, it is interesting to note that allowing the wing geometry to be optimized as well results in 7-10% improvements of relative mission range over the same case with a fixed wing geometry. This shows that while the use of credibility in the optimization can be applied to any aircraft design to provide an interesting evaluation of risk for performance benefit, other changes with less development risk might actually provide larger benefits. Thus, the implementation of credibility-based optimization presented in this paper is best applied to a previously optimized airframe.

For all curves, lower credibility limits imply better component performance for all considered parameters. Improved performance is mostly represented in smaller and lighter components. As the MTOMs are active constraints, the

overall aircraft design doesn't change. Improvements in range are mainly a result of transporting more total energy for the mission, in larger batteries and more available mission fuel, filling up the remaining mass allowance. Further improvements are gained through a trade off between fuel and battery mass as battery energy density increases for lower credibility levels.

However, even though the effect of varying credibility on achievable range seems straightforward, the relative importance between the individual components at different credibility levels is more complex and investigated in detail in the following paragraphs. Component trade-offs show sensitivity to both the component's current actual mass, and the underlying credibility curves determining the rate of mass improvements for credibility changes.

The table 3 shows the corresponding aircraft mass breakdowns for the most restricted case, only varying the energy network parameters. It can be seen that the results for all four credibility levels have a very similar breakdown for their MTOM, wing and structural masses. For lower credibilities, the motor mass is consistently decreasing, while the fuel mass is increasing. As the installed motor power is related to the MTOM through a power-to-weight ratio, with an increase in the gravimetric energy density, the motor becomes lighter for similar power ratings. Due to the whole electrical system getting lighter and the batteries being more efficient, more fuel can be uplifted by the aircraft, increasing its range. The resulting battery mass is a result of the two other factors. At high credibility values (shifting from 90% to 70% credibility), the large decreases in motor mass are due to the underlying Weibull distribution of the parameter. This decrease in motor mass allows the aircraft to take more battery and fuel mass onboard to keep the same total MTOM. For further reductions in credibility, higher battery energy density allows larger ranges despite reductions in the actual battery mass. Mass reductions in the other parameters are used to carry more fuel to support the batteries in achieving the higher ranges as well. For the low 30% credible results, the battery mass is again decreasing compared to the 50% credible results, although more energy is stored on the aircraft.

Table 3 Mass breakdown of the optimized regional jet at different credibility levels for the network parameter only (Battery Gravimetric Energy Density (BGE), Electric Motor Gravimetric Power Density (EMG), Electric Motor Volumetric Power Density (EMV)) optimization

Parameter	Reference	30% Cred	50% Cred	70% Cred	90% Cred
MTOM [kg]	33024	33026	33045	33086	33029
Structure [kg]	7335	7331	7334	7339	7337
Wing [kg]	2685	2683	2685	2691	2688
Motor [kg]	1202	480	450	507	714
Battery [kg]	8243	8868	8965	8999	8851
Fuel [kg]	1595	1695	1643	1586	1483

Investigating the resulting component credibility and performance values in table 4 shows that the battery energy density always converges to the highest allowable performance value. The credibility values shown in parenthesis in the table have always converged to the lower limit of 10% less than the specified average level. Similar to the previous

aircraft design, the battery proves to be the dominant performance driver. The electrical motor shows the behavior discussed in the previous paragraph. For high credibilities, the improvement in performance to the next lower data point is larger than for low credibility values. The volumetric power density is a tertiary component for all optimizations. The main parameters have an influence on the mass of the aircraft, not the performance.

Table 4 Resulting component performance and credibility levels of regional jet for given average credibility and network parameter only (BGE, EMG, EMV) optimization

Parameter	Reference	30% Cred	50% Cred	70% Cred	90% Cred
BGE [Wh/kg]	543.4 (12%)	532 (20%)	513 (40%)	496 (60%)	476 (80%)
EMG [kW/kg]	4.0 (99%)	11.1 (34%)	10.4(45%)	9.5 (60%)	6.7 (91%)
EMV [kW/l]	35.2 (31%)	33.7 (36%)	26.0 (65%)	16.1 (90%)	8.3 (98%)

When the airframe parameters are also included in the optimization problem, the results change in magnitude and shape. Firstly, the influence of the wing weight reductions becomes visible in the wing and structural masses in table 5. The lower the credibility, the lower the mass. The motor, battery, and fuel masses show clear trends. Again the motor mass improvements are the largest mass-wise when comparing high credibility data points. Both fuel and battery mass increase for lower credibilities. The reduction in wing and motor mass now allows the batteries and fuel volume to be larger compared to the previous, more constrained case. This benefit directly translates to a higher achievable range.

Table 5 Mass breakdown of the optimized regional jet at different credibility levels for all uncertain parameters (NLF, Structural Weight Reductions (SWR), BGE, EMG, EMV) optimization

Parameter	Reference	30% Cred	50% Cred	70% Cred	90% Cred
MTOM [kg]	33024	33046	33094	33026	33026
Structure [kg]	7334	6919	7008	7083	7182
Wing [kg]	2685	2270	2359	2434	2533
Motor [kg]	1202	403	451	582	621
Battery [kg]	8243	9309	9299	9130	9058
Fuel [kg]	1595	1756	1676	1583	1519

The observation that both motor and wing masses have the highest absolute reductions at high credibilities, is also visible for the relative changes in table 6. The exponential distribution used to model the structural weight reductions is well visible. For the 90% credible case, the parameter is barely used due to the large reduction in credibility that a small improvement would yield. An initial improvement of the parameter of 3% requires a reduction in credibility from of 30%, whereas an improvement of a further 3% would only require a less than 20% further reduction in credibility.

Utilizing all five uncertain parameters, the relative importance also shifts. The battery is still the dominant parameter, but now the relative importance of the electric motor has become more pronounced than in the previous optimization. Regarding the parameters having an influence on the aerodynamic performance of the aircraft, the optimal laminar flow

results seem to lie in the region of 38-40% of the wing. All optimizations (30%, 50%, 70%) where this result was within the bounds of the optimizer converged to similar values for the laminar flow. Only the 90% credible aircraft shows a significantly lower value due to its lower bound limitations. The volumetric power density of the machines shows a low influence at high credibility values, and even at lower allowable credibility data points, it is never a limiting (or close to limiting) value. Hence, again the volumetric power density shows to be of low importance to the final aircraft design.

Table 6 Resulting component performance and credibility levels of regional jet for given average credibility and all uncertain parameter (NLF, SWR, BGE, EMG, EMV) optimization

Parameter	Reference	30% Cred	50% Cred	70% Cred	90% Cred
NLF [%]	0 (100%)	38.9 (57%)	40.2 (53%)	37.8 (60%)	23.7 (90%)
SWR [%]	12 (31%)	12.2 (29%)	10.7(43%)	7.45 (62%)	4.55 (99%)
BGE [Wh/kg]	543 (12%)	533 (20%)	513 (40%)	496 (60%)	476 (80%)
EMG [kW/kg]	4.0 (99%)	11.95 (20%)	10.68 (40%)	8.26 (78%)	7.73 (83%)
EMV [kW/l]	35.2 (31%)	32.9 (39%)	23.0 (73%)	8.0 (96%)	5.0 (99%)

Lastly, including the wing geometry as three additional design variables shows some interesting effects. The new parameters are Aspect Ratio (AR), taper ratio (λ) and leading edge sweep angle (Λ). Similar to the previous case, without wing optimization, wing structure and motor mass show a monotonous decrease in mass for a decrease in average credibility as shown in table 7.

Due to the allowable wing variations, an additional constraint was included, the mission fuel burn must be equal to or lower than the fuel burns reported in table 5. This constraint became necessary due to the optimization framework set-up shown in fig. 5. By constraining the maximum allowable wing span, and iterating around a given design wing and thrust loading, the aircraft can converge to a very low aspect ratio design. This allows a large increase in wing area before the span constraint becomes active with a corresponding increase in allowable MTOM. Thus, the final aircraft will be very heavy and thus capable of carrying a large amount of fuel and batteries, but be aerodynamically much less efficient than the baseline. This is an undesired effect, and thus a constraint on fuel efficiency was added.

The addition of this constraint, in combination with the optimized wing geometry, resulted in more efficient aircraft. The design point was kept constant, and thus the installed engine thrust and motor power were constant. The reduction in fuel mass indicates that improvements in aerodynamic efficiency reduced the required thrust throughout the flight. This corresponds to higher battery masses. As the boost power was kept as a constant fraction of the installed power, a more efficient airframe corresponds to longer flight ranges and hence heavier batteries.

Comparing the credibility results in table 8, it can be seen that now both battery and wing weight parameters have become dominant, whereas the motor mass becomes less limiting for low credibility levels. The level of laminar flow has a varying impact on the final design. For the 90% credible case, mass parameters are absolutely dominating the design. For credibilities of 50% and less, a larger application of laminar flow brings performance benefits. This

Table 7 Mass breakdown of the optimized regional jet at different credibility levels for all parameters and wing geometry (NLF, SWR, BGE, EMG, EMV, AR, λ, Λ) optimization

Parameter	Reference	30% Cred	50% Cred	70% Cred	90% Cred
MTOM [kg]	33024	33046	33051	33020	33026
Structure [kg]	7334	6791	6911	6977	7030
Wing [kg]	2685	2163	2258	2329	2373
Motor [kg]	1202	467	485	506	598
Battery [kg]	8243	9755	9580	9374	9562
Fuel [kg]	1595	1390	1431	1518	1206

shows that at high credibility levels when the uncertain parameter performance is most limited, the largest benefits are achieved by reducing the total aircraft mass and thus allowing more fuel and batteries to be taken aboard. If the credibility constraints are relaxed, the mass parameters are already at good levels, and a further increase in gravimetric density would only yield a small relative improvement for a larger reduction in credibility. At this level, the performance influencing parameters start becoming more relevant for further improvements. However, they are always of lower importance than mass reductions.

Table 8 Resulting component performance and credibility levels of regional jet for given average credibility and all uncertain parameter plus wing geometry (NLF, SWR, BGE, EMG, EMV, AR, λ, Λ) optimization

Parameter	Reference	30% Cred	50% Cred	70% Cred	90% Cred
NLF [%]	0 (100%)	50 (27%)	44 (40%)	25 (82%)	10 (99%)
SWR [%]	12 (31%)	13.4 (24%)	10.3 (40%)	7.4 (62%)	4.4 (99%)
BGE [Wh/kg]	543.4 (12%)	531 (21%)	514 (40%)	496 (60%)	476 (80%)
EMG [kW/kg]	4.0 (99%)	10.3 (47%)	9.9 (53%)	9.5 (60%)	8.1 (80%)
EMV [kW/l]	35.2 (31%)	25 (66%)	20.0 (77%)	14.8 (92%)	15.4 (91%)
AR	8.43	7.6	7.99	7.89	7.52
λ	0.32	0.29	0.35	0.37	0.43
Λ_{LE}	25.44	18.3	16.9	20.7	23.8

The changes in the wing geometry show that a lower aspect ratio of the wing is desired. The interactions of wing weight reductions, laminar flow, and taper seem to correlate; and the optimal taper ratio decreases for a lower credibility limit. Both taper and aspect ratio have an influence on the distribution of the aerodynamic load, and thus, the required wing mass. For this flight condition, the optimal wing also has a lower sweep angle than the reference aircraft. As the credibility for laminar flow is a function of the sweep angle and wing Reynolds number and changes in these parameters have a direct impact on the laminar flow results. As such, the optimal area of laminar flow increases from 38-40% to 44-50% of the wing for a less swept design, with a corresponding increase in aerodynamic efficiency that manifested itself in the lower total fuel burn while flying a longer range. The design changes of the wing geometry are graphically

shown in fig. 13, compared to the original wing design.

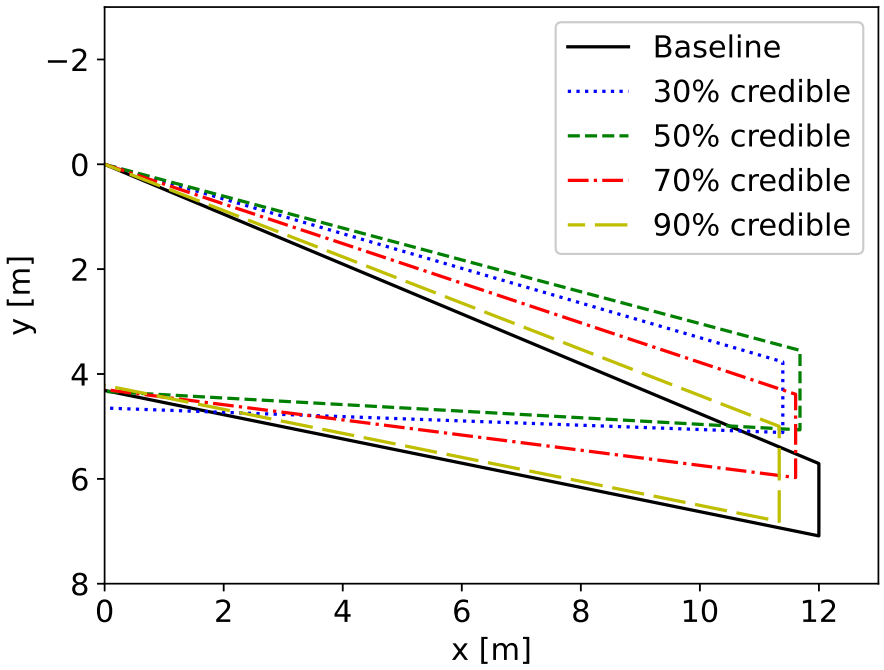

Fig. 13 Optimized wing planform geometries of the regional jet for average credibilities

B. CS-23 19-Passenger Fully-Electric Commuter Aircraft

The second case study aircraft features 19 seats and is certified under EASA CS-23 certification specifications [63]. The aircraft has an aluminum structure and two electric motors that are powered by a battery assembly stored in the main wing. The aircraft is created by the Initiator [62], a conceptual aircraft design tool, with industry-accepted performance figures for its energy network and shown in fig. 14 with design parameters presented in table 9. The aircraft is specifically designed to be at the corner of the CS-23 limits and to investigate the limits of this certification specification for electric aviation. It has a no-reserves mission range of 237 NM (440 km). This shows how challenging this aircraft configuration can be, with a severely limited potential market. Hence, improvements in the network performance and reductions in specific battery mass are of the utmost importance for this aircraft concept, to achieve higher mission ranges and create a commercially viable design.

The aircraft is converted into the SUAVE format retaining the same performance requirements and design point. The mission is approximated by discretization of the flight phases. As the Initiator models aircraft designs based on reference aircraft constructions, the wing is sized as aluminum construction. With an increase in the use of composites in wing designs of state-of-the-art aircraft, a composite wing structure will most likely be a primary choice for next generation aircraft of all sizes. The credibility assessment regarding structural weight reductions works on assumed

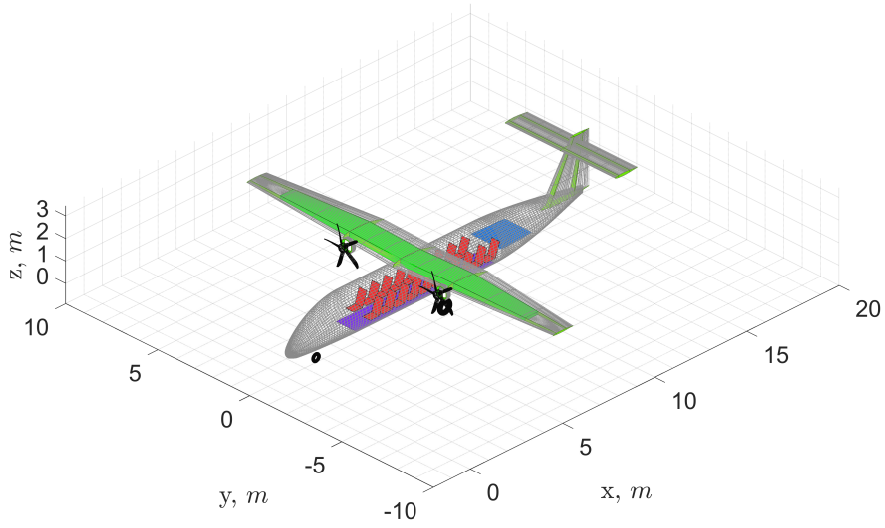

Fig. 14 CS-23 19-passenger fully-electric commuter aircraft baseline design

improvements in composite tailoring techniques. Thus, in the modeling of the SUAVE aircraft, a conversion factor is implemented to account for the weight savings of a composite wing over an aluminum structure [34].

Table 9 Key design parameter of the 19-passenger commuter for the optimization

Parameter	Value
Wing loading	2712 N/m^2
Power loading	0.0948 N/W
Number of passengers	19
Cruise speed	113.75 m/s
Cruise altitude	3658 m
Wing aspect ratio	9
Wing taper ratio	0.45
Wing sweep	0°

For CS-23 aircraft, the MTOM is limited to 6818 kg [63]. Thus, the wingspan constraint from eq. (8) is replaced by a mass constraint, resulting in the optimization problem shown in eq. (10). Optimization is again performed for four levels of average credibility, 30%, 50%, 70%, and 90%. For each individual component credibility, the limit was set to 10% less than the prescribed average.

$$
\begin{aligned}
min \quad & -R_{mission} \\
s.t. \quad & MTOM \leq MTOM_{max,CS23} \\
& C_i \geq C_{i,limit} \qquad \forall i = 1, 2, ..., n \\
& \frac{1}{n}\sum_{n=1}^{i} C_i \geq C_{avg,limit}
\end{aligned}
\tag{10}
$$

The average credibility constraint is created to force a trade-off between the different uncertain parameters while keeping the limiting values close to the desired average. The result will be an aircraft where the most influential parameters have credibility levels below the average while less influential parameters are above. This approach is well suited to investigate the relative importance of the parameters between each other. However, one goal of this optimization is to evaluate the performance increases against the increase in development risk. For this, a multiplicative criterion is better suited. The total credibility (C_{total}) defined in eq. (11) can be used to quantify the total credibility (or risk) of a given aircraft design.

$$
C_{total} = \Pi_{n=1}^{i} C_i \tag{11}
$$

This multiplication of the individual credibilities ensures that the total performance risk is accounted for in the constraints. This constraint formulation prevents highly influential parameters from resulting in very low credibility while keeping every other parameter at very high credibility and thus obscuring the true performance risk with an unrealistic average. In the total credibility criterion, the most ambitious parameter always drives the attainable credibility, while preventing highly ambitious values due to the presence of multiple parameters. Due to the multiplication, it is also highly sensitive to the number of uncertain parameters used in the evaluation, and comparisons can only be made for optimizations using the same uncertain parameters. However, it allows to remove all constraints on individual component credibility in the optimization problem as it is specifically designed to not have the weaknesses of an average. Hence the updated optimization formulation using total credibility can be seen in eq. (12).

$$
\begin{aligned}
min \quad & -R_{mission} \\
s.t. \quad & MTOM \leq MTOM_{max,CS23} \\
& \Pi_{n=1}^{i} C_i \geq C_{tot,limit}
\end{aligned}
\tag{12}
$$

The effects of this criterion compared to the average criterion are shown in fig. 15. As the total criterion results in

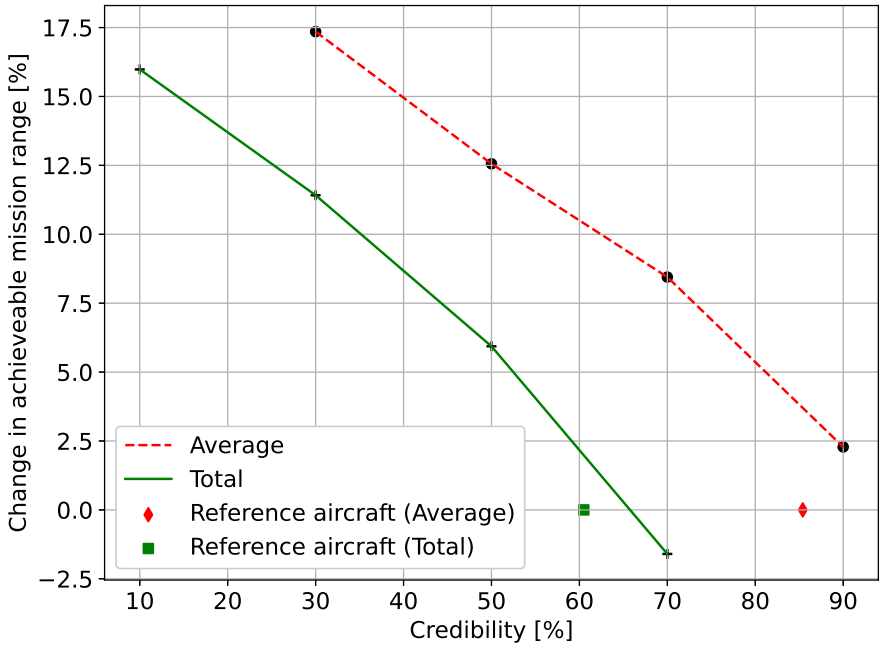

Fig. 15 Credibility-mission range Pareto front curves for the fully-electric 19-passenger commuter optimizations

low values, while component credibilities are relatively high, the curve is shifted to show a range of 10% to 70% total credibility. This shift results in component credibilities for the most limiting parameter to a similar range as the average cases of a 20% higher limit. The reference aircraft is represented with two points due to the difference in credibility when assessed by the average or total criterion. The respective colors match the reference aircraft to the corresponding credibility curve. The resulting curves show better performance at the respective credibilities compared to the reference design. The reference uses realistic input values from current literature, but is not optimized for performance and credibility yet.

The curves show a decreasing performance gain for each subsequent step in reducing credibility. Even higher credibility results for the average curve show improvements over the baseline design, with further increases of 15% in range over the investigated credibility range. The total credibility curve shows the more limiting nature of this criterion. While the optimized results show an improvement over the baseline, the initial point is close to the optimized curve and higher total credibility results show a lower performance. However, the total relative improvement over the full credibility range is higher than in the average case.

The previous subsection utilized all uncertain parameters in their optimization and concluded that the network parameters are more influential than the airframe parameters, especially for higher credibilities. This set of optimizations focuses on the energy network and has a closer look at its effects on mission performance. Thus, the airframe parameters

are not used for this aircraft. The mass results shown in table 10 reflect this by showing very similar values for wing and structural masses. The electric motor mass shows a decreasing trend, with the largest change having a 30% reduction in mass when moving from 90% to 70% credibility, and only a further 10% per step in limiting credibility. A reason for this difference is the high limiting credibility in the 90% case where a direct trade-off in performance with the battery energy density is forced. Thus, the change between the two highest credibility limits is larger than for every subsequent step. The mass savings due to the motor as well are directly invested in the battery mass, to increase the achievable mission range.

In the motor gravimetric power density results, again the underlying credibility function shape is well visible. A steep decrease from 90% to 60% component credibility for the 90% and 70% average credible cases respectively corresponds with a large increase in component performance and corresponding reduction in component mass. Further reductions in credibility (past 50%) show a shallowing slope on the respective CF (fig. 1), and as such further mass reductions are of smaller magnitude.

Table 10 Mass breakdown of optimized 19-passenger commuter at different average credibility levels for the network parameter only (BGE, EMG, EMV) optimization

Parameter	Reference	30% Cred	50% Cred	70% Cred	90% Cred
MTOM [kg]	8593	8618	8620	8624	8629
Structure [kg]	1916	1956	1956	1956	1956
Wing [kg]	747	786	786	786	786
Motor [kg]	323	122	135	152	213
Battery [kg]	3100	3248	3237	3224	3168

The forced trade-off for the motor for the 90% credible design is very well visible in the component credibility levels shown in table 11. The 30% to 70% credible results show a clear parameter hierarchy. Both battery energy density and motor gravimetric power density are dominant over a reduction in motor volumetric power density. Removing the airframe parameters from the optimization problem thus shows a very obvious optimum. For the 90% credible design, the hierarchy between the battery and motor is shown clearly. Thus, for an average limiting criterion, the hierarchical order for the network parameters is: batteries, motor mass, and motor volume.

Table 11 Resulting component performance and credibility levels of 19-passenger commuter for given average credibility and network parameter only (BGE, EMG, EMV) optimization

Parameter	Reference	30% Cred	50% Cred	70% Cred	90% Cred
BGE [Wh/kg]	486 (71%)	533 (20%)	513 (40%)	496 (60%)	476 (80%)
EMG [kW/kg]	4.0 (99%)	11.9 (20%)	10.7 (40%)	9.50 (60%)	6.78 (91%)
EMV [kW/l]	18.2 (86%)	29.8 (50%)	24.0 (70%)	16.1 (90%)	5 (99%)

Investigating the results of the total credibility in table 12, it can be seen that while the general trends are the same

compared to the previous results, now the motor has a larger performance change at low credibilities, while having comparatively high masses at higher credibilities. The battery mass is still increasing, although at lower ranges than the average case, and with a much flatter slope for range improvement at lower credibilities.

Table 12 Mass breakdown of optimized 19-passenger commuter at different total credibility levels for the network parameter only (BGE, EMG, EMV) optimization

Parameter	Reference	10% Cred	30% Cred	50% Cred	70% Cred
MTOM [kg]	8593	8596	8595	8593	8595
Structure [kg]	1916	1916	1916	1916	1916
Wing [kg]	747	747	747	747	747
Motor [kg]	323	151	180	190	193
Battery [kg]	3100	3274	3246	3233	3230

This effect of lower performance can also be seen in the component credibilities in table 13. The battery performance is again a clear driving force, always reaching values within 10% of the total limit. This severely limits improvements in the motor performance, with values for both parameters around 90% credible or more. It is interesting to note that in contrast to the previous optimization, now the volumetric power density is also used more actively, such as for the 50% result where it has a lower credibility than the gravimetric result. However, overall both parameters are of secondary importance to the battery performance. Only for the 10% credible case show the motor parameters some notable improvement, with values in the 70s for both. The data shows that while the battery performance dominates the results, for each credibility level there is a point at which improvements in the motor performance are more advantageous overall than a further change in battery energy density. Thus, while the previous study showed a clear hierarchical order, the motor parameters retain an eventual relevance for further performance gains.

Table 13 Resulting component performance and credibility levels of 19-passenger commuter for given total credibility and network parameter only (BGE, EMG, EMV) optimization

Parameter	Reference	10% Cred	30% Cred	50% Cred	70% Cred
BGE [Wh/kg]	486 (71%)	534 (19%)	517 (35%)	494 (62%)	476 (80%)
EMG [kW/kg]	4.0 (99%)	8.54 (74%)	7.20 (88%)	6.80 (91%)	6.52 (93%)
EMV [kW/l]	18.2 (86%)	23.74 (71%)	7.51 (99%)	17.0 (88%)	13.1 (95%)

VI. Conclusions

This paper presents a novel approach to optimization under uncertainty in the time domain. By using credibility curves to assess the future performance of key design parameters, it is to add a layer of chance-of-realization to the necessary assumptions regarding future network performance. The proposed credibility criterion assesses the probability that at a specified time a certain technology will have reached at least a certain performance level. For five uncertain

performance parameters, probability distributions were fitted to represent the probability of performance levels for 2035, from which the resulting credibility distributions can be directly extracted. A surrogate-based global optimization framework based on Gaussian Process (GP) and using an Expected Improvement (EI) infill criterion is created and verified, both on the optimization algorithm and full model integration level.

A set of credibility-based optimizations is performed on a Boosted-Turbofan (BTF) CS-25 regional jet using a wingspan limit as defining geometric constraint. Credibility results are obtained for using just the energy network parameters, using all uncertain parameters, and using all parameters and a variable wing geometry. Results show benefits of approx. 17% when optimizing for all uncertain parameters compared to optimizing just for the network parameters. For the optimization cases with all uncertain parameters, the laminar flow results show consistently that approx. 50% Natural Laminar Flow (NLF) is an optimal point. For this aircraft, changes in the wing geometry to lower aspect ratio and sweep angles resulted in a further 20% benefit over the fixed geometry case. This shows that the initial aircraft design was not yet fully optimized. While changes in wing sweep have a direct effect on the credibility results for the laminar flow parameter, the overall wing changes and resulting performance gains show that the pure geometry optimization have the larger effect. The credibility-based optimization thus can be used both in the design optimization phase and as a second step on a finalized design to investigate the sensitivity of the chosen uncertain parameters.

A second set of credibility-based optimizations of a fully electric CS-23 aircraft for maximum mission range is performed, using credibility and the CS-23 mass limit as constraints. Results obtained for an average credibility criterion are similar to the previous case, and consolidate the notion of a hierarchical structure in the importance of network parameters. The batteries are the most limiting, followed by the gravimetric motor power. The volumetric power density has only a small influence on the total achievable mission range. Results obtained using a multiplicative total credibility criterion show similar results as well as a reduction in mission range due to the stricter requirements.

The total credibility criterion is better suited for assessing the overall design credibility of a proposed concept. However, its bounds and interpretation must be handled with care as the results depend strongly on the amount of design variables. The average criterion is more robust regarding changing amounts of design variables, but it requires individual credibilities to be constrained to sensible minimum values to prevent on-average credible, yet unrealistic results. It is thus best suited as a sensitivity criterion to assess the relative impact of parameters and their credibility functions amongst each other.

The methodology of defining credibility and using it as a measure of performance risk estimation is easily scalable and applicable to virtually all (sub-) components of an engineering design. A limited number of parameters is chosen for this study. However, the developed software is capable to include any number of parameters, provided sufficient computational power is given and sufficient data for a credibility curve generation can be found.

Factors influencing computational costs are the complexity of the underlying models and the optimization algorithm. Simple models and surrogates can allow increased problem sizes. In more complex designs, the choice of an appropriate

optimization algorithm is of increasing importance. Most important is the availability, quality and accuracy of the underlying performance prediction data. Prognostic data found in literature is usually scarce and hence different approaches to credibility curve creation might be required. The performed studies show, however, that the problem can be solved to some degree by incorporating different types of distribution functions, depending on the type of available data. The choice of distribution function can be a limiting factor. Due to low data availability, statistical curve-fitting tests have limited accuracy, hence the final choice of ideal distribution is both dependent on mathematical results and engineering judgment.

The idea of combining probability functions, describing the development of state-of-the-art technology, with a design optimizer is shown to be a promising concept. Although aircraft design was chosen as the application example, the method can be transferred to other technological fields, applying the developed statistical methods and functions. Advantages of applying the credibility measure can be especially imagined to explore design spaces where new technologies are investigated. Also, one can think of advantages in the support of management decisions, e.g. the quantification of investment risks.

Acknowledgments

This research is part of the Credible HYbrid-eLectric Aircraft (CHYLA) project and has received funding from the Clean Sky 2 Joint Undertaking (JU) under grant agreement No 101007715. The JU receives support from the European Union's Horizon 2020 research and innovation program and the Clean Sky 2 JU members other than the Union.

The authors wish to thank Vincent Bonnin and Maurice Hoogreef from the Department of Aerodynamics, Wind Energy, Flight Performance and Propulsion of the Aerospace Engineering Faculty of Delft University of Technology for the provided baseline aircraft design and performance figures used in this publication.

References

[1] Airbus SAS, *Global Market Forecast, Cities, Airports & Aircraft 2019-2038*, Airbus SAS, 2019.

[2] Directorate General for Research and Innovation, Directorate General for Mobility and Transport, *Flightpath 2050: Europe's Vision for Aviation*, European Commission, 2011.

[3] Karpuk, S., and Elham, A., "Influence of novel airframe technologies on the feasibility of fully-electric regional aviation," *Aerospace*, Vol. 8, No. 6, 2021, p. 163. https://doi.org/https://doi.org/10.3390/aerospace8060163.

[4] Bowman, C., Felder, J., and Marien, T., "Turbo-and hybrid-electrified aircraft propulsion concepts for commercial transport," *2018 AIAA/IEEE Electric Aircraft Technologies Symposium (EATS)*, AIAA, 2018. https://doi.org/https://doi.org/10.2514/6.2018-4984.

[5] Sahoo, S., Zhao, X., and Kyprianidis, K., "A review of concepts, benefits, and challenges for future electrical propulsion-based aircraft," *Aerospace*, Vol. 7, No. 4, 2020, p. 44. https://doi.org/https://doi.org/10.3390/aerospace7040044.

[6] Finger, D., Braun, C., and Bil, C., "Comparative assessment of parallel-hybrid-electric propulsion systems for four different aircraft," *Journal of Aircraft*, Vol. 57, No. 5, 2020, pp. 843–853. https://doi.org/https://doi.org/10.2514/1.C035897.

[7] Hoelzen, J., Liu, Y., Bensmann, B., Winnefeld, C., Elham, A., Friedrichs, J., and Hanke-Rauschenbach, R., "Conceptual design of operation strategies for hybrid electric aircraft," *Energies*, Vol. 11, No. 1, 2018, p. 217. https://doi.org/https://doi.org/10.3390/en11010217.

[8] Liu, Y., Elham, A., Horst, P., and Hepperle, M., "Exploring vehicle level benefits of revolutionary technology progress via aircraft design and optimization," *Energies*, Vol. 11, No. 1, 2018, p. 166. https://doi.org/https://doi.org/10.3390/en11010166.

[9] Cinar, G., Cai, Y., Bendarkar, M. V., Burrell, A. I., Denney, R. K., and Mavris, D. N., "System analysis and design space exploration of regional aircraft with electrified powertrains," *Journal of Aircraft*, Vol. 60, No. 2, 2023, pp. 382–409. https://doi.org/https://doi.org/10.2514/1.C036919.

[10] Brelje, B., and Martins, J., "Electric, hybrid, and turboelectric fixed-wing aircraft: A review of concepts, models, and design approaches," *Progress in Aerospace Sciences*, Vol. 104, 2019, pp. 1–19. https://doi.org/https://doi.org/10.1016/j.paerosci.2018.06.004.

[11] Thomson, R., Sachdeva, N., Nazukin, M., and Martinez, N., "Aircraft Electrical Propulsion–The Next Chapter of Aviation?" *Think: Act*, 2017, pp. 1–32.

[12] Thomson, R., Baum, M., Kirschstein, T., Martinez, N., Sachdeva, N., Lepine, P., and Bailly, N., "Aircraft Electrical Propulsion – Onwards and Upwards," *Think: Act*, 2018, pp. 1–32.

[13] ICAO Committee on Aviation Environmental Protection, "Report on the Feasibility of a Long-term Aspirational Goal (LTAG) for International Civil Aviation CO2 Emission Reductions," Tech. rep., International Civil Aviation Organization, 2022.

[14] ICAO Committee on Aviation Environmental Protection, "Report on the Feasibility of a Long-term Aspirational Goal (LTAG) for International Civil Aviation CO2 Emission Reductions - Appendix M3 LTAG-TG Technology Sub Group Report," Tech. rep., International Civil Aviation Organization, 2022.

[15] Wahler, N., Radomsky, L., Hanisch, L., Mallwitz, R., Henke, M., and Elham, A., "A credibility-based criterion for the assessment of futuristic aircraft concepts," *33rd Congress of the International Council of the Aeronautical Sciences*, International Council of the Aeronautical Sciences, 2022.

[16] Matheron, G., "Kriging or polynomial interpolation procedures," *Canadian Institute of Mining and Metallurgy Transactions*, Vol. 70, No. 1, 1967, pp. 240–244.

[17] Forrester, A., Sobester, A., and Keane, A., *Engineering design via surrogate modelling: a practical guide*, John Wiley & Sons, 2008. https://doi.org/https://doi.org/10.1002/9780470770801.

[18] Jones, D., Schonlau, M., and Welch, W., "Efficient global optimization of expensive black-box functions," *Journal of Global optimization*, Vol. 13, No. 4, 1998, pp. 455–492. https://doi.org/https://doi.org/10.1023/A:1008306431147.

[19] Jiao, R., Zeng, S., Li, C., Jiang, Y., and Jin, Y., "A complete expected improvement criterion for Gaussian process assisted highly constrained expensive optimization," *Information Sciences*, Vol. 471, 2019, pp. 80–96. https://doi.org/https://doi.org/10.1016/j.ins.2018.09.003.

[20] Hoogreef, M. F., Radomsky, L., Henke, M., Friedrich, J., Wahler, N. F., and Elham, A., "Credible HYbrid eLectric Aircraft deliverable D2.1: Report on top-level aircraft requirements (TLAR) and matrix of technologies," Tech. rep., European Union Clean Sky 2, 2020.

[21] Löbberding, H., Wessel, S., Offermanns, C., Kehrer, M., Rother, J., Heimes, H., and Kampker, A., "From cell to battery system in BEVs: Analysis of system packing efficiency and cell types," *World Electric Vehicle Journal*, Vol. 11, No. 4, 2020, pp. 1–15. https://doi.org/https://doi.org/10.3390/wevj11040077.

[22] Mueller, J.-K., Bensmann, A., Bensmann, B., Fischer, T., Kadyk, T., Narjes, G., Kauth, F., Ponick, B., Seume, J., and Krewer, U., "Design considerations for the electrical power supply of future civil aircraft with active high-lift systems," *Energies*, Vol. 11, No. 1, 2018, p. 179. https://doi.org/https://doi.org/10.3390/en11010179.

[23] Tiede, B., O'Meara, C., and Jansen, R., "Battery Key Performance Projections based on Historical Trends and Chemistries," *2022 IEEE Transportation Electrification Conference & Expo (ITEC)*, Institute of Electrical and Electronics Engineers, 2022, pp. 754–759. https://doi.org/https://doi.org/10.1109/ITEC53557.2022.9814008.

[24] Heidmann, J., "NASA Investments in Hybrid-Electric Technologies for Large Commercial Aircraft," *NASA Glenn Research Center, Electric & Hybrid Aerospace Technology Symposium*, NASA, 2015.

[25] Bird, J., "A Review of Electric Aircraft Drivetrain Motor Technology," *IEEE Transactions on Magnetics*, Vol. 58, No. 2, 2022, pp. 1–8. https://doi.org/10.1109/TMAG.2021.3081719.

[26] Mitchell, B., "A comparison of chi-square and Kolmogorov-Smirnov tests," *Area*, Vol. 3, No. 4, 1971, pp. 237–241.

[27] Stodieck, O., Cooper, J., Weaver, P., and Kealy, P., "Aeroelastic tailoring of a representative wing box using tow-steered composites," *AIAA journal*, Vol. 55, No. 4, 2017, pp. 1425–1439. https://doi.org/https://doi.org/10.2514/1.J055364.

[28] Tatting, B., Gürdal, Z., and Jegley, D., "Design and manufacture of elastically tailored tow placed plates," Tech. Rep. NASA/CR-2002-211919, NASA, 2002.

[29] Stodieck, O., Cooper, J., Weaver, P., and Kealy, P., "Improved aeroelastic tailoring using tow-steered composites," *Composite Structures*, Vol. 106, 2013, pp. 703–715. https://doi.org/https://doi.org/10.1016/j.compstruct.2013.07.023.

[30] Stanford, B., and Jutte, C., "Comparison of curvilinear stiffeners and tow steered composites for aeroelastic tailoring of aircraft wings," *Computers & Structures*, Vol. 183, 2017, pp. 48–60. https://doi.org/https://doi.org/10.1016/j.compstruc.2017.01.010.

[31] Stanford, B., Jutte, C., and Wieseman, C., "Trim and structural optimization of subsonic transport wings using nonconventional aeroelastic tailoring," *AIAA Journal*, Vol. 54, No. 1, 2016, pp. 293–309. https://doi.org/https://doi.org/10.2514/1.J054244.

[32] Jutte, C., Stanford, B., Wieseman, C., and Moore, J., "Aeroelastic tailoring of the NASA common research model via novel material and structural configurations," *52nd aerospace sciences meeting*, AIAA, 2014. https://doi.org/https://doi.org/10.2514/6.2014-0598.

[33] Brooks, T., Kennedy, G., and Martins, J., "High-fidelity aerostructural optimization of a high aspect ratio tow-steered wing," *57th AIAA/ASCE/AHS/ASC Structures, Structural Dynamics, and Materials Conference*, AIAA, 2016. https://doi.org/https://doi.org/10.2514/6.2016-1179.

[34] Soutis, C., "Fibre reinforced composites in aircraft construction," *Progress in aerospace sciences*, Vol. 41, No. 2, 2005, pp. 143–151. https://doi.org/https://doi.org/10.1016/j.paerosci.2005.02.004.

[35] Nelson, W., "Composite wing conceptual design," Tech. Rep. AFML-TR-73-57, Douglas Aircraft Co., 1973.

[36] Joslin, R., "Aircraft laminar flow control," *Annual review of fluid mechanics*, Vol. 30, No. 1, 1998, pp. 1–29. https://doi.org/https://doi.org/10.1146/annurev.fluid.30.1.1.

[37] Krishnan, K., Bertram, O., and Seibel, O., "Review of hybrid laminar flow control systems," *Progress in Aerospace Sciences*, Vol. 93, 2017, pp. 24–52. https://doi.org/https://doi.org/10.1016/j.paerosci.2017.05.005.

[38] Green, J., "Laminar flow control-back to the future?" *38th Fluid Dynamics Conference and Exhibit*, AIAA, 2008. https://doi.org/https://doi.org/10.2514/6.2008-3738.

[39] Horstmann, K., Redeker, G., Quast, A., Dressler, U., and Bieler, H., "Flight tests with a natural laminar flow glove on a transport aircraft," *Flight Simulation Technologies Conference and Exhibit*, AIAA, 1990. https://doi.org/https://doi.org/10.2514/6.1990-3044.

[40] Riedel, H., Horstmann, K.-H., Ronzheimer, A., and Sitzmann, M., "Aerodynamic design of a natural laminar flow nacelle and the design validation by flight testing," *Aerospace science and technology*, Vol. 2, No. 1, 1998, pp. 1–12. https://doi.org/https://doi.org/10.1016/S0034-1223(98)80001-8.

[41] Collier, J., "An overview of recent subsonic laminar flow control flight experiments," *23rd Fluid Dynamics, Plasmadynamics, and Lasers Conference*, AIAA, 1993. https://doi.org/https://doi.org/10.2514/6.1993-2987.

[42] Fujino, M., Yoshizaki, Y., and Kawamura, Y., "Natural-laminar-flow airfoil development for a lightweight business jet," *Journal of Aircraft*, Vol. 40, No. 4, 2003, pp. 609–615. https://doi.org/https://doi.org/10.2514/2.3145.

[43] Seitz, A., Hübner, A., and Risse, K., "The DLR TuLam project: design of a short and medium range transport aircraft with forward swept NLF wing," *Council of European Aerospace Socienties Aeronautical Journal*, Vol. 11, No. 2, 2020, pp. 449–459. https://doi.org/https://doi.org/10.1007/s13272-019-00421-1.

[44] Hanks, G., "Natural Laminar flow airfoil analysis and trade studies," Tech. Rep. NASA/CR-159029, NASA, 1979.

[45] Schmitt, V., Archambaud, J., Horstmann, K., and Quast, A., "Hybrid laminar fin investigations," *NATO Applied Vehicle Technology Panel Symposium Braunschweig, 08.-11.05.2000*, NATO, 2000.

[46] Schrauf, G., and von Geyr, H., "Simplified hybrid laminar flow control for the A320 fin-Aerodynamic and system design, first results," *AIAA Scitech 2020 Forum*, AIAA, 2020. https://doi.org/https://doi.org/10.2514/6.2020-1536.

[47] Fischer, M., Wright JR, A., and Wagner, R., "A flight test of laminar flow control leading-edge systems," *Aircraft Design, Systems and Technology Meeting*, AIAA, 1983. https://doi.org/https://doi.org/10.2514/6.1983-2508.

[48] Bhutiani, P., Keck, D., Lahti, D., and Stringas, M., "Investigating the merits of a hybrid laminar flow nacelle," *The Leading Edge*, 1993, pp. 32–35.

[49] Beck, N., Landa, T., Seitz, A., Boermans, L., Liu, Y., and Radespiel, R., "Drag reduction by laminar flow control," *Energies*, Vol. 11, No. 1, 2018, p. 252. https://doi.org/https://doi.org/10.3390/en11010252.

[50] Karpuk, S., Liu, Y., and Elham, A., "Multi-fidelity design optimization of a long-range blended wing body aircraft with new airframe technologies," *Aerospace*, Vol. 7, No. 7, 2020, p. 87. https://doi.org/https://doi.org/10.3390/aerospace7070087.

[51] Sudhi, A., Elham, A., and Badrya, C., "Coupled Boundary-Layer Suction and Airfoil Optimization for Hybrid Laminar Flow Control," *AIAA Journal*, Vol. 59, No. 12, 2021, pp. 5158–5173. https://doi.org/https://doi.org/10.2514/1.J060480.

[52] Reneaux, J., and Blanchard, A., "The design and testing of an airfoil with hybrid laminar flow control," *1st European Forum on Laminar Flow Technology*, Office national d'études et de recherches aérospatiales, 1992, pp. 164–174.

[53] Schmitt, V., Reneaux, J., and Priest, J., "Maintaining laminarity by boundary Layer control," *1992 Scientific and Technical Activities*, 1993, pp. 13–14.

[54] Chernyshev, S., Kiselev, A., and Kuryachii, A., "Laminar flow control research at TsAGI: Past and present," *Progress in Aerospace Sciences*, Vol. 47, No. 3, 2011, pp. 169–185. https://doi.org/https://doi.org/10.1016/j.paerosci.2010.11.001.

[55] Wahler, N., Maruyama, D., and Elham, A., "Credibility-Based Multidisciplinary Design Optimisation of Electric Aircraft," *AIAA SCITECH 2023 Forum*, AIAA, 2023. https://doi.org/https://doi.org/10.2514/6.2023-1847.

[56] Hepperle, M., "Electric Flight - Potential and Limitations," *NATO Applied Vehicle Technology-209 Workshop on Energy Efficient Technologies and Concepts Operations*, NATO, 2012.

[57] Schrauf, G., "Status and perspectives of laminar flow," *The aeronautical journal*, Vol. 109, No. 1102, 2005, pp. 639–644. https://doi.org/https://doi.org/10.1017/S000192400000097X.

[58] Sobol, I., "On the distribution of points in a cube and the approximate evaluation of integrals," *Zhurnal Vychislitel'noi Matematiki i Matematicheskoi Fiziki*, Vol. 7, No. 4, 1967, pp. 784–802. https://doi.org/https://doi.org/10.1016/0041-5553(67)90144-9.

[59] Botero, E., Wendorff, A., MacDonald, T., Variyar, A., Vegh, J., Lukaczyk, T., Alonso, J., Orra, T., and Ilario da Silva, C., "Suave: An open-source environment for conceptual vehicle design and optimization," *54th AIAA Aerospace Sciences Meeting*, AIAA, 2016. https://doi.org/https://doi.org/10.2514/6.2016-1275.

[60] Wahler, N., Radomsky, L., Hanisch, L., Göing, J., Meyer, P., Mallwitz, R., Friedrichs, J., Henke, M., and Elham, A., "An Integrated Framework for Energy Network Modeling in Hybrid-Electric Aircraft Conceptual Design," *AIAA AVIATION 2022 Forum*, AIAA, 2022. https://doi.org/https://doi.org/10.2514/6.2022-3741.

[61] MacDonald, T., Clarke, M., Botero, E., Vegh, J., and Alonso, J., "SUAVE: an open-source environment enabling multi-fidelity vehicle optimization," *18th AIAA/ISSMO Multidisciplinary Analysis and Optimization Conference*, AIAA, 2017. https://doi.org/https://doi.org/10.2514/6.2017-4437.

[62] Elmendorp, R., Vos, R., and La Rocca, G., "A conceptual design and analysis method for conventional and unconventional airplanes," *ICAS 2014: Proceedings of the 29th Congress of the International Council of the Aeronautical Sciences, St. Petersburg, Russia, 7-12 September 2014*, International Council of Aeronautical Sciences, 2014.

[63] European Aviation Safety Agency, *Easy Access Rules for Normal-Category Aeroplanes (CS-23)(CS Amendment 5, AMC/GM Issue 2)*, European Aviation Safety Agency, 2018.